

Cavity Moiré Materials: Controlling magnetic frustration with quantum light-matter interaction

Kanta Masuki*

Department of Physics, University of Tokyo, 7-3-1 Hongo, Bunkyo-ku, Tokyo 113-0033, Japan

Yuto Ashida†

Department of Physics, University of Tokyo, 7-3-1 Hongo, Bunkyo-ku, Tokyo 113-0033, Japan and

Institute for Physics of Intelligence, University of Tokyo, 7-3-1 Hongo, Tokyo 113-0033, Japan

Cavity quantum electrodynamics (QED) studies the interaction between light and matter at the single quantum level and has played a central role in quantum science and technology. Combining the idea of cavity QED with moiré materials, we theoretically show that strong quantum light-matter interaction provides a way to control frustrated magnetism. Specifically, we develop a theory of moiré materials confined in a cavity consisting of thin polar van der Waals crystals. We show that nontrivial quantum geometry of moiré flat bands leads to electromagnetic vacuum dressing of electrons, which produces appreciable changes in single-electron energies and manifests itself as long-range electron hoppings. We apply our general formulation to a twisted transition metal dichalcogenide heterobilayer encapsulated by ultrathin hexagonal boron nitride layers and predict its phase diagram at different twist angles and light-matter coupling strengths. Our results indicate that the cavity confinement enables one to control magnetic frustration of moiré materials and might allow for realizing various exotic phases such as a quantum spin liquid.

I. INTRODUCTION

Controlling exotic phases of matter has been an ongoing quest in condensed matter physics. Moiré materials are emerging platforms for studying strongly correlated phenomena, where a long-periodic moiré pattern is formed by two overlaid crystal layers with relative twists or different lattice constants. Such moiré superlattice induces reconstruction of electronic structures and realizes nearly flat bands at certain twist angles [1–3]. In flat-band systems, the kinetic energy of electrons is significantly suppressed and the effect of electron-electron interaction becomes important [4, 5]. So far, a number of intriguing phenomena have been experimentally observed in twisted bilayer graphene [6–8], including metal-insulator transition [9–11], flat-band superconductivity [12–16], magnetism [17–20], and fractional quantum Hall effect [21–24]. Owing to rapid advances in manipulation of van der Waals (vdW) heterostructures [25, 26], moiré materials consisting of transition metal dichalcogenides (TMDs) have also been extensively investigated [27–39]. In particular, the high tunability of TMDs enables one to study various correlated phases [40–51] and might allow for realizing exotic states such as a quantum spin liquid (QSL) [52–55].

On another front, experimental developments in cavity quantum electrodynamics (QED) have allowed for realizing the ultrastrong coupling regime, where light-matter interaction is comparable to elementary excitation energies [56–68]. Recent studies have discussed the cavity confinement as an alternative way to control the phase

of matter without an external drive in a wide variety of fields, including quantum optics [69–74], polaritonic chemistry [75–78], and condensed matter physics [79–90]. In particular, the possibility of controlling certain material properties, such as topological aspects [91–96], superconductivity [97–101], correlated phenomena [102–106], and Landau polaritons [107–113], has been so far explored. On the one hand, due to the smallness of the fine structure constant, the single-quantum ultrastrong coupling is out of reach in a usual Fabry-Perot cavity consisting of metallic mirrors [114]. On the other hand, this difficulty can be overcome by employing hybridization with matter excitations. For instance, a recent study [115] has shown that a new cavity geometry, in which two ultrathin vdW layers form a planar cavity, can achieve single-quantum ultrastrong couplings and thus provides an ideal platform to explore ultrastrong coupling physics of two-dimensional electronic materials. There, an optical anisotropy in vdW layers leads to the formation of phonon polaritons having hyperbolic dispersion [116]. The electrons are then strongly coupled to tightly confined hyperbolic polaritons, where the coupling strength can be tuned simply by changing thicknesses of vdW slabs. Given these developments and prospects, it is natural to address whether or not the cavity confinement enables one to control correlated phases of moiré materials.

In this paper, taking a step beyond Ref. [115], we show that strong quantum light-matter interaction provides a way to control many-body properties of moiré materials. Specifically, we develop a theory of cavity moiré materials to describe the interaction between electrons in a twisted bilayer and quantized electromagnetic fields inside a cavity (Fig. 1(a)) and show that magnetic frustration in moiré materials can be controlled by the cavity confinement. A key point is that, unlike isolated

* masuki@g.ecc.u-tokyo.ac.jp

† ashida@phys.s.u-tokyo.ac.jp

flat-band systems, moiré materials are inherently multi-band systems with large interlayer contributions in tensor Berry connections [117, 118]. We show that this quantum geometric effect causes vacuum-induced virtual electronic transitions between flat bands and the other bands, leading to the renormalization of single-electron energies in flat bands. While such vacuum-induced modification is usually irrelevant in conventional materials, we point out that it becomes important in moiré materials because of their extremely narrow bandwidths.

We demonstrate that this electromagnetic vacuum dressing allows for controlling a variety of correlated phases of moiré materials, some of which remain elusive in current experiments. Specifically, we apply our theory to a TMD moiré heterobilayer encapsulated by ultrathin hexagonal boron nitride (*h*-BN) slabs (Fig. 1(a)), where light-matter coupling strength η can be tuned by varying *h*-BN thicknesses. At small twist angle θ and half-filling, low-energy physics of the flat-band electrons can be described by the spin-1/2 antiferromagnetic (AFM) Heisenberg model on the triangular moiré lattice [28, 94, 119]. When placed inside the cavity, vacuum fluctuations appreciably renormalize the single-electron energies and induce long-range electron hoppings. As a result, the cavity confinement enhances the spin frustration in the Heisenberg model and allows one to control various phases including the 120°-AFM phase and the zigzag phase (Fig. 1(b)). Notably, in the intermediate regions, one may even realize a QSL phase of the triangular Heisenberg model, whose nature has been recently under debate [120–125]. We expect that these predictions are within experimental reach owing to recent developments demonstrating ultrasmall mode volumes of hyperbolic polaritons in nanostructured materials [126–131].

The rest of this paper is organized as follows. In Sec. II,

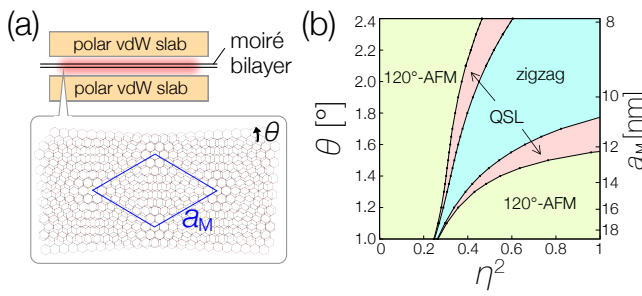


FIG. 1. (a) Schematic figure of cavity moiré materials. Electrons in a moiré bilayer are ultrastrongly coupled to hyperbolic phonon polaritons confined in the cavity consisting of polar vdW crystals such as *h*-BN. The bottom panel shows a moiré superlattice with lattice constant a_M formed by a bilayer with twist angle θ . (b) Ground-state phase diagram of the cavity-confined TMD heterobilayer at half-filling plotted against θ and dimensionless light-matter coupling strength η^2 . Tuning η and θ , one can control various correlated phases, such as the 120°-antiferromagnetic (AFM) phase, the zigzag phase, and a candidate quantum spin liquid (QSL) phase.

we introduce the total Hamiltonian to describe moiré materials confined in hyperbolic cavities. In Sec. III, we derive the low-energy effective Hamiltonian of flat-band electrons by performing the perturbative analysis, which is one of the main results of this paper. Importantly, the effect of the cavity confinement is represented by the dressing of single-electron energies of the flat band. In Sec. IV, we examine the general properties of the effective Hamiltonian and show that the energy-dressing of flat-band electrons enhances the long-range couplings in real space, whose characteristic length scale can be controlled by the light-matter coupling strength and the twist angle of moiré materials. Lastly, in Sec. V, we employ our formalism to analyze the spin-ground state of flat-band electrons in WSe₂/MoSe₂. Our results indicate that the cavity confinement enables one to control the magnetic frustration of moiré materials and might allow for realizing various many-body phases. Section VI summarizes the results and discusses the future directions for non-perturbative analysis of cavity moiré materials. Some technical details are discussed in Appendix.

II. MODEL DESCRIPTION

To be concrete, we focus on a cavity confinement of twisted TMD heterobilayer WSe₂/MoSe₂, while our theoretical formulation can be generally applied to other moiré materials (see Appendix A for details). Due to the spin-orbit coupling, the valence bands of each monolayer have two band maxima at different valleys with opposite spin degrees of freedom (Fig. 2(a)) [28, 133]. Since the valence band maxima (VBM) of monolayer WSe₂ are located in the band gap of MoSe₂, we can analyze the bilayer in terms of the VBM electrons in WSe₂ provided that the chemical potential is tuned near the VBM of WSe₂ (red dashed line in Fig. 2(a)) [3, 28, 134].

When the TMD bilayer is twisted with small angle θ , a triangular moiré superlattice with lattice constant $a_M \approx a_0/\theta$ is formed (see Fig. 1(a)), where $a_0 \simeq 3.32$ Å is the monolayer lattice constant of WSe₂. The effect of the moiré superlattice can be described by an effective single-particle potential $\Delta(\mathbf{r})$, which has the same periodicity as the moiré superlattice [3, 28]. The low-energy Hamiltonian of the VBM electrons thus reads

$$\hat{H}_0 = -\frac{\hat{\mathbf{p}}^2}{2m^*} + \Delta(\hat{\mathbf{r}}), \quad (1)$$

where m^* is the effective mass in the valence band of WSe₂, and the moiré potential $\Delta(\mathbf{r})$ is given by

$$\Delta(\mathbf{r}) = \sum_{j=1}^6 w_j e^{i\mathbf{b}_j \cdot \mathbf{r}}. \quad (2)$$

Here, \mathbf{b}_j is the reciprocal lattice vector of the moiré superlattice corresponding to $(j-1)\pi/3$ -rotation of $4\pi/(\sqrt{3}a_M)\mathbf{e}_x$. Since $\Delta(\mathbf{r})$ is real-valued and satisfies the

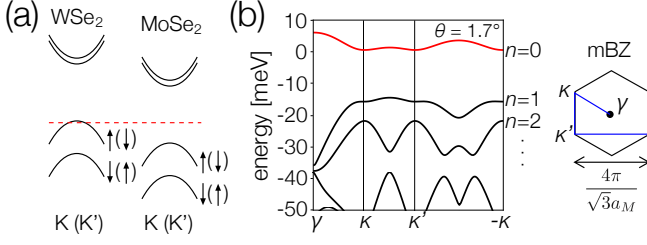


FIG. 2. (a) Schematic band dispersions of monolayer WSe₂ and MoSe₂. The valence band maxima (VBM) of WSe₂ at different valleys with the opposite spin are located in the band gap of MoSe₂. The red dashed line represents the Fermi level. (b) Moiré bands of Eq. (1) at $\theta = 1.7^\circ$. The nearly flat band with $n = 0$ is highlighted by red color. The right panel shows representative points on the moiré Brillouin zone (mBZ). Parameters are $(w, \psi) = (6.6 \text{ meV}, -94^\circ)$ and $m^* = 0.35m_e$, where m_e is the electron mass [28].

threefold-rotational symmetry, the coefficients w_j can be parametrized as $w_j = we^{-i(-1)^j\psi}$.

In Fig. 2(b), we show typical band dispersions $\varepsilon_{n\mathbf{k}}$ of the moiré Hamiltonian (1) on the moiré Brillouin Zone (mBZ), where one can see the nearly flat band ($n = 0$) located above the other bands ($n \geq 1$). It is noteworthy that, due to the nontrivial quantum geometry of the moiré flat band, the electron momentum $\hat{\mathbf{p}}$ has nonvanishing interband matrix elements between the flat band and the other bands below, while the innerband matrix element of $\hat{\mathbf{p}}$ within the flat band almost vanishes due to the band flatness [117, 118]. Since electrons couple to the dynamical electromagnetic fields with vector potential \mathbf{A} through $\hat{\mathbf{p}} \cdot \mathbf{A}$, it is these nonvanishing matrix elements that facilitate the couplings between flat-band electrons and cavity fields as detailed below.

The total Hamiltonian of the cavity-confined bilayer is given by minimally coupling the vector potential operator of cavity fields $\hat{\mathbf{A}}$ to the momentum operator of electrons $\hat{\mathbf{p}}$. In the second-quantized form, the total Hamiltonian is expressed as

$$\hat{H} = \sum_{\sigma} \int d^2\mathbf{r} \hat{\psi}_{\sigma\mathbf{r}}^{\dagger} \left[-\frac{(-i\hbar\nabla + e\hat{\mathbf{A}}(\mathbf{r}))^2}{2m^*} + \Delta(\mathbf{r}) \right] \hat{\psi}_{\sigma\mathbf{r}} + \sum_{\mathbf{q}} \hbar\omega_{\mathbf{q}} \hat{a}_{\mathbf{q}}^{\dagger} \hat{a}_{\mathbf{q}} + \hat{U}, \quad (3)$$

where we also include the Coulomb interaction \hat{U} . Here, $\hat{\psi}_{\sigma\mathbf{r}}$ ($\hat{\psi}_{\sigma\mathbf{r}}^{\dagger}$) is the annihilation (creation) operator of electrons with spin σ at position \mathbf{r} , $\hat{a}_{\mathbf{q}}$ ($\hat{a}_{\mathbf{q}}^{\dagger}$) is the annihilation (creation) operator of hyperbolic polaritons with in-plane momentum \mathbf{q} , and $\omega_{\mathbf{q}}$ is the mode frequency. The vector potential $\hat{\mathbf{A}}(\mathbf{r})$ is

$$\hat{\mathbf{A}}(\mathbf{r}) = \sum_{\mathbf{q}} A_{\mathbf{q}} \mathbf{e}_{\mathbf{q}} (\hat{a}_{\mathbf{q}} e^{i\mathbf{q}\mathbf{r}} + \hat{a}_{\mathbf{q}}^{\dagger} e^{-i\mathbf{q}\mathbf{r}}), \quad (4)$$

where $A_{\mathbf{q}}$ is the mode amplitude of the electromagnetic component of polaritons, and $\mathbf{e}_{\mathbf{q}} \equiv \mathbf{q}/|\mathbf{q}|$ is the effec-

tive polarization obtained after projecting the originally transverse 3D vector field onto the 2D plane where the bilayer is located. We define the integrated dimensionless coupling strength η by

$$\eta \equiv \sqrt{\sum_{\mathbf{q}} g_{\mathbf{q}}^2 / \omega_{\mathbf{q}}^2}, \quad (5)$$

where $g_{\mathbf{q}}$ is the coupling strength between electrons and each cavity mode defined as

$$g_{\mathbf{q}} \equiv e A_{\mathbf{q}} \sqrt{\omega_{\mathbf{q}} / m^* \hbar}. \quad (6)$$

The value of η can reach up to $\eta \sim 1$ provided that thicknesses of h-BN slabs are tuned to be a few nanometers [115]. Lastly, we note that the phonon loss in vdW materials can in principle affect the mode amplitudes and the coupling strength of the hyperbolic phonon polaritons. However, as described in Appendix D, its effect is expected to be negligibly small in hyperbolic polaritons of h-BN.

III. EFFECTIVE HAMILTONIAN OF FLAT-BAND ELECTRONS

We are now in a position to derive the effective Hamiltonian of flat-band electrons. To this end, we first note that the cavity frequency, which is an order of optical phonon frequency in vdW crystals $\hbar\omega_{\mathbf{q}} = 10^2 \sim 10^3$ meV, is much larger than band gaps in the twisted bilayer (cf. Fig. 2(b)). Therefore, the low-energy states of cavity moiré Hamiltonian (3) can be approximated by a product state $|\psi_e\rangle \otimes |0\rangle$, where $|0\rangle$ is the electromagnetic vacuum, and $|\psi_e\rangle$ is an electronic state with the partially filled flat band and occupied lower electronic bands (cf. Fig. 3(a)). We can then adiabatically eliminate the cavity modes and include their vacuum fluctuations by performing the perturbative analysis with respect to η .

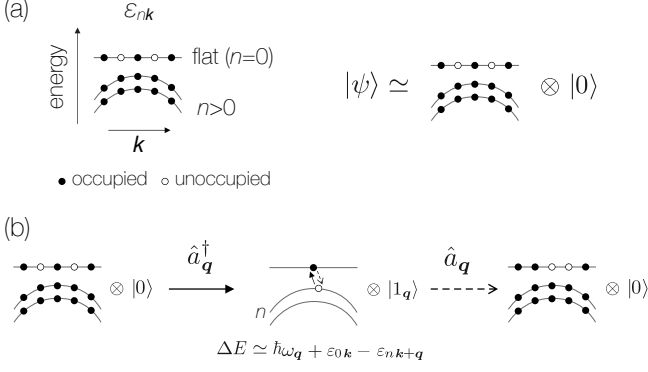
As detailed in Appendix A, the leading contributions come from the second-order perturbation of the paramagnetic interaction term

$$\hat{H}_I^{(p)} = \sum_{\sigma} \int d^2\mathbf{r} \hat{\psi}_{\sigma\mathbf{r}}^{\dagger} \left[\frac{i\hbar e(\nabla \cdot \hat{\mathbf{A}}(\mathbf{r}) + \hat{\mathbf{A}}(\mathbf{r}) \cdot \nabla)}{2m^*} \right] \hat{\psi}_{\sigma\mathbf{r}} \quad (7)$$

$$= - \sum_{\mathbf{q}\mathbf{k}\sigma} \sum_{mn} \frac{eA_{\mathbf{q}}}{\hbar} (\mathbf{G}_{mn}^{k,q} \cdot \mathbf{e}_{\mathbf{q}}) \hat{c}_{m\mathbf{k}+\mathbf{q}\sigma}^{\dagger} \hat{c}_{n\mathbf{k}\sigma} \hat{a}_{\mathbf{q}} + \text{H.c.}, \quad (8)$$

where $\hat{c}_{n\mathbf{k}\sigma}^{(\dagger)}$ is the annihilation (creation) operator of n -th band electrons with the Bloch wavevector \mathbf{k} and spin σ . Also, we introduce the multiband coefficients \mathbf{G}_{mn}^k by

$$\mathbf{G}_{mn}^k \equiv \langle u_{m\mathbf{k}} | \nabla_{\mathbf{k}} \hat{H}_{0\mathbf{k}} | u_{n\mathbf{k}} \rangle, \quad (9)$$



where $|u_{n\mathbf{k}}$ is the Bloch eigenstate of $\hat{H}_{0\mathbf{k}} \equiv e^{-i\mathbf{k}\hat{\mathbf{r}}} \hat{H}_0 e^{i\mathbf{k}\hat{\mathbf{r}}}$ with band index n . Using simplifications that are valid in moiré flat-band systems, we obtain the effective Hamiltonian of cavity moiré materials, which is one of the main results in this paper (see Appendix A for detailed derivations):

$$\hat{H}_{\text{eff}} = \sum_{\mathbf{k}\sigma} (\varepsilon_{0\mathbf{k}} + \eta^2 \xi_{\mathbf{k}}) \hat{c}_{\mathbf{k}\sigma}^\dagger \hat{c}_{\mathbf{k}\sigma} + \hat{U}, \quad (10)$$

$$\xi_{\mathbf{k}} \equiv \frac{m^*}{2\hbar^2} \left(-|\mathbf{G}_{00}^{\mathbf{k}}|^2 + \sum_{n \geq 1} \frac{\hbar\omega_0}{\hbar\omega_0 + \varepsilon_{0\mathbf{k}} - \varepsilon_{n\mathbf{k}}} |\mathbf{G}_{0n}^{\mathbf{k}}|^2 \right). \quad (11)$$

Here, we abbreviate the creation (annihilation) operator of flat-band electrons $\hat{c}_{0\mathbf{k}\sigma}^{(\dagger)}$ as $\hat{c}_{\mathbf{k}\sigma}^{(\dagger)}$. Remarkably, the effect of light-matter interactions is simply represented by the energy dressing $\eta^2 \xi_{\mathbf{k}}$ characterized by the multiband coefficients $\mathbf{G}_{mn}^{\mathbf{k}}$. We note that the last term in the right hand side of Eq. (11) originates from the second-order perturbation process that simultaneously excites electrons below the flat band and cavity modes and then annihilates them (cf. Fig 3(b)). We note that the vacuum fluctuations in the cavity also mediate the Amperean electron-electron interaction in general. However, since its coefficients are proportional to $(\mathbf{G}_{00}^{\mathbf{k},\mathbf{q}} \cdot \mathbf{e}_{\mathbf{q}})(\mathbf{G}_{00}^{\mathbf{k}',\mathbf{q}^*} \cdot \mathbf{e}_{\mathbf{q}}) \approx (\nabla_{\mathbf{k}} \varepsilon_{0\mathbf{k}} \cdot \mathbf{e}_{\mathbf{q}})(\nabla_{\mathbf{k}} \varepsilon_{0\mathbf{k}'} \cdot \mathbf{e}_{\mathbf{q}})$, the Amperean interaction is negligibly small compared to the Coulomb interaction \hat{U} (see Appendix A).

From a quantum geometrical viewpoint, the multiband coefficients $\mathbf{G}_{mn}^{\mathbf{k}}$ (9) can be expressed as

$$\mathbf{G}_{mn}^{\mathbf{k}} = \delta_{mn} \nabla_{\mathbf{k}} \varepsilon_{n\mathbf{k}} + i(\varepsilon_{m\mathbf{k}} - \varepsilon_{n\mathbf{k}}) \mathcal{A}_{mn}(\mathbf{k}) \quad (12)$$

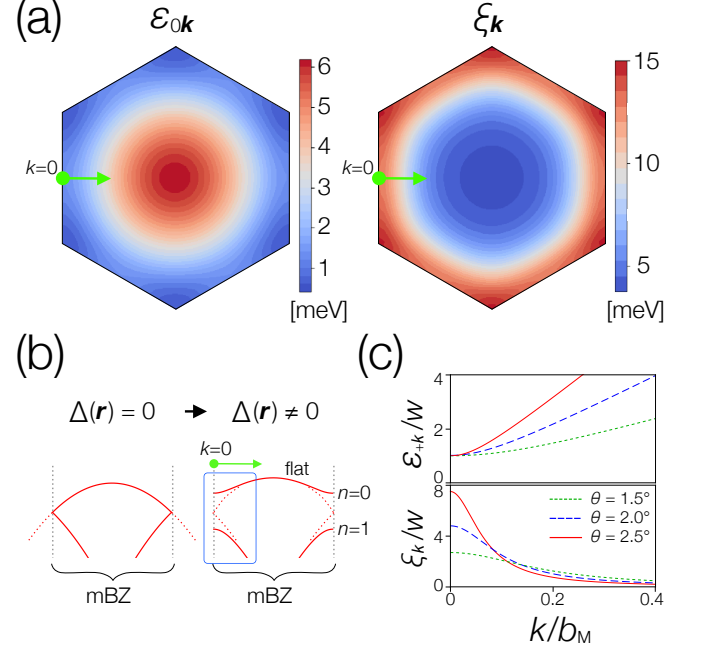


FIG. 4. (a) Typical moiré flat-band dispersion $\varepsilon_{0\mathbf{k}}$ (left panel) and cavity renormalization $\xi_{\mathbf{k}}$ in Eq. (11) (right panel) on the mBZ with $\theta = 1.7^\circ$ and $\hbar\omega_0 = 10^2$ meV. (b) Schematic figure illustrating the formation of the moiré flat band. (c) Band dispersion $\varepsilon_{i,k}/W$ and cavity renormalization $\xi_{\mathbf{k}}$ (Eqs. (14) and (15)) of the two-band Hamiltonian (13) plotted against k/b_M with $b_M = 4\pi/(\sqrt{3}a_M)$, where $k=0$ corresponds to the edge of the mBZ as indicated in (a) and (b).

with $\mathcal{A}_{mn}(\mathbf{k}) = i\langle u_{m\mathbf{k}} | \nabla u_{n\mathbf{k}} \rangle$ being the tensor Berry connections. In moiré materials, \mathcal{A}_{mn} has large interband contributions, while $\nabla_{\mathbf{k}} \varepsilon_{0\mathbf{k}}$ vanishes in the flat-band limit [117, 118]. Thus, the renormalization $\xi_{\mathbf{k}}$ in Eq. (11) is mainly attributed to its second term originating from virtual interband transitions induced by the vacuum fluctuations in the cavity. Also, due to the flatness of the moiré electronic band, the dispersion of the renormalization $\xi_{\mathbf{k}}$ in Eq. (10) becomes larger than the original band dispersion $\varepsilon_{0\mathbf{k}}$. As detailed in Sec. V, this feature of cavity moiré materials allows one to control ground-state magnetic properties of flat-band electrons. We note that these key multiband processes in moiré materials cannot be captured in an oversimplified description of cavity materials, such as the Peierls substitution of the single-band tight-binding model.

IV. GENERAL PROPERTIES IN CAVITY MOIRÉ MATERIALS

To reveal generic features of cavity moiré materials, in Fig. 4(a) we show typical bare dispersion $\varepsilon_{0\mathbf{k}}$ of the nearly flat band and the corresponding cavity renormalization $\xi_{\mathbf{k}}$ on the mBZ. Interestingly, the dispersions of $\varepsilon_{0\mathbf{k}}$ and $\xi_{\mathbf{k}}$ are opposite each other, namely, $\varepsilon_{0\mathbf{k}}$ ($\xi_{\mathbf{k}}$) takes the

largest value at the center (edge) of the mBZ. Moreover, the contributions of $\xi_{\mathbf{k}}$ are tightly localized around the edge of the mBZ, which can be translated to the emergence of long-range electron hoppings in real-space basis.

To understand these key features, we first note that the coefficient, $\hbar\omega_0/(\hbar\omega_0 + \varepsilon_{0\mathbf{k}} - \varepsilon_{n\mathbf{k}})$, in the renormalization $\xi_{\mathbf{k}}$ in Eq. (11) monotonically decreases with respect to the band index n , and the cavity dressing $\xi_{\mathbf{k}}$ is mainly attributed to electronic bands with small n . Therefore, the behavior of $\varepsilon_{0\mathbf{k}}$ and $\xi_{\mathbf{k}}$ can be qualitatively understood by analyzing a simple two-band model for moiré electronic bands with $n = 0, 1$. In the TMD bilayer, the original monolayer band around VBM is first folded into the mBZ (left panel in Fig. 4(b)) in accordance with the change of the lattice constant from a_0 to a_M . The degeneracy at the edge of the mBZ is then lifted by the moiré potential $\Delta(\mathbf{r})$, leading to the nearly flat moiré band (right panel in Fig. 4(b)). We can thus describe the energy bands near the mBZ edge by the following two-band Hamiltonian:

$$\mathcal{H}(k) = \hbar v_F k \hat{\sigma}_z + w \hat{\sigma}_x, \quad (13)$$

where $\hat{\sigma}_i$ is the Pauli matrix, k is the wavevector measured from the edge of the mBZ, v_F is the Fermi velocity at the mBZ edge (cf. left panel in Fig. 4(b)), and $w = |w_j|$ is the depth of the moiré potential in Eq. (2). Using the two-band model (13), the energy dispersions $\varepsilon_{\pm k}$ and the cavity renormalization ξ_k can be obtained as

$$\varepsilon_{\pm k} = \pm w \sqrt{1 + \left(\frac{\hbar v_F k}{w}\right)^2}, \quad (14)$$

$$\xi_k = \frac{m^* v_F^2}{1 + \left(\frac{\hbar v_F k}{w}\right)^2} + \text{const.} \quad (15)$$

As shown in Fig. 4(c), ε_{+k} (ξ_k) takes the smallest (largest) value at the edge of the mBZ, which correctly reproduces the qualitative features in Fig. 4(a). Also, ξ_k in Eq. (15) is localized around $k = 0$ with a width $\Delta k \sim w/(\hbar v_F) \propto \theta^{-1}$ (cf. Fig. 4(c)). In real space, this leads to a long-distance hopping whose range is proportional to θ . In general, such long-range contribution can generate strong magnetic frustration and is expected to qualitatively affect the ground-state properties as discussed below.

V. TIGHT-BINDING DESCRIPTION AND THE SPIN MODEL

Using the Wannier basis, we can rewrite the effective Hamiltonian (10) by the following Hubbard model on the

moiré triangular lattice:

$$\hat{H}_{\text{eff}} = \sum_{ij,\sigma} t_{ij} \hat{c}_{i\sigma}^\dagger \hat{c}_{j\sigma} + U \sum_i \hat{n}_{i\uparrow} \hat{n}_{i\downarrow}, \quad (16)$$

$$t_{ij} = \int_{\text{mBZ}} \frac{v_M d^2 \mathbf{k}}{(2\pi)^2} (\varepsilon_{0\mathbf{k}} + \eta^2 \xi_{\mathbf{k}}) e^{i\mathbf{k}(\mathbf{R}_i - \mathbf{R}_j)} \quad (17)$$

$$\equiv \tilde{\varepsilon}_{ij} + \eta^2 \tilde{\xi}_{ij}, \quad (18)$$

where $\hat{c}_{i\sigma}^{(\dagger)}$ is the annihilation (creation) operator of the Wannier orbital localized at \mathbf{R}_i , v_M is the volume of the moiré supercell, and we simplify the Coulomb repulsion by the on-site interaction $U \sum_i \hat{n}_{i\uparrow} \hat{n}_{i\downarrow}$ [28]. Let us represent the hoppings t_{ij} to the n -th nearest neighbors (NNs) by t_n and neglect the amplitudes t_n with $n \geq 4$, which are sufficiently small when $\theta \lesssim 2.5^\circ$. Since the parameters satisfy $t_n \ll U$ [28], at half-filling, we can further simplify the Hubbard model (16) to the triangular AFM Heisenberg model [119]:

$$\hat{H}_{\text{AFM}} = \sum_{\text{1st NN}} J_1 \hat{s}_i \cdot \hat{s}_j + \sum_{\text{2nd NN}} J_2 \hat{s}_i \cdot \hat{s}_j + \sum_{\text{3rd NN}} J_3 \hat{s}_i \cdot \hat{s}_j, \quad (19)$$

where \hat{s}_i is the spin-1/2 operator at the i -th site, and $J_n \equiv 4t_n^2/U$. This frustrated spin model has been studied in, e.g., Refs. [121–125], and a nonmagnetic insulating phase, which is a candidate QSL phase, is found in the parameter region around $J_2/J_1 \sim 0.3$ and $J_3/J_1 \sim 0.15$ [122].

One of our main findings is the possibility of controlling such spin frustration by the cavity confinement. Specifically, one can tune the light-matter coupling strength η to enhance the hopping amplitudes t_n to distant sites ($n = 2, 3$) while suppressing the NN hopping t_1 (Fig. 5(b)). Physically, this tunability originates from the opposite dispersions in $\varepsilon_{0\mathbf{k}}$ and $\xi_{\mathbf{k}}$ described above (Fig. 4(a)), which correspond to the opposite signs of their Fourier transforms, $\tilde{\varepsilon}_n$ and $\tilde{\xi}_n$, that are related to the renormalized hopping via $t_n = \tilde{\varepsilon}_n + \eta^2 \tilde{\xi}_n$. We show the corresponding η -dependence of J_2/J_1 and J_3/J_1 in Fig. 5(c), where one can realize particularly large spin-coupling ratios J_n/J_1 when the NN coupling J_1 becomes vanishingly small. Comparing with the numerical results in the triangular AFM Heisenberg model [122], we determine the ground-state phase diagram of the present cavity moiré system as in Fig. 1(b). The key finding is that the high tunability of η and θ should allow for controlling various correlated phases including a candidate QSL phase.

VI. DISCUSSIONS AND CONCLUSIONS

We recall that a central feature of cavity moiré materials is the renormalization of single-electron energies in flat bands, which is induced by the virtual interband transitions originating from the nontrivial quantum geometry of moiré bands (cf. Eqs. (11) and (12)). While vacuum fluctuations can also induce the Amperean

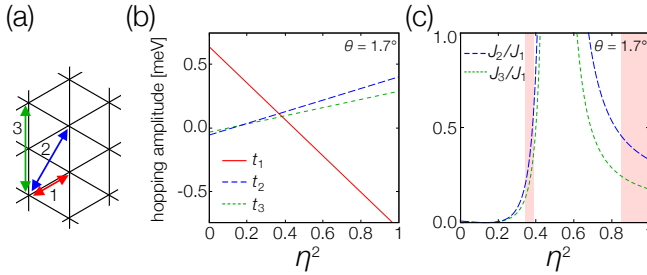


FIG. 5. (a) First-, second-, and third-order nearest neighbors (NNs) on the moiré triangular lattice. (b) Renormalized hopping amplitudes t_n to the n -th NNs and (c) corresponding spin-coupling ratios J_i/J_1 ($i = 2, 3$) in the triangular AFM Heisenberg model (19) plotted against the light-matter coupling strength at $\theta = 1.7^\circ$. The red shaded areas in (c) indicate the intermediate parameter regions where the ground state is expected to be a quantum spin liquid.

electron-electron interaction [98], we note that this contribution is negligibly small compared to the Coulomb interaction due to the flatness of moiré bands as detailed in Appendix A. In contrast, a usual monolayer has dispersive bands and band gap is typically much larger than a resonance frequency of the *h*-BN cavity considered here. Thus, if monolayer is confined in the vdW slabs, the Amperean paring term could be also relevant.

In summary, we developed a theory of moiré materials strongly coupled to quantized electromagnetic fields inside a cavity. We showed that the major effect of the cavity confinement is the renormalization of the single-electron energies in flat bands. Physically, this originates from the nontrivial quantum geometry of the moiré bands, which leads to virtual interband electronic transitions induced by electromagnetic vacuum fluctuations. The resulting long-range electronic hoppings allow for tuning the spin frustration in the low-energy effective model, thus suggesting the possibility of controlling correlated phases with quantum light-matter interaction. We analyzed the concrete setup consisting of TMD heterobilayer WSe₂/MoSe₂ confined in the *h*-BN cavity, and revealed that various phases, including a putative QSL state, can be realized by varying the light-matter coupling strength η (Fig. 1(b)).

Ultimately, a further nonperturbative analysis should be necessary to fully assess the validity of our predictions in the relevant interaction strength regime in Fig. 1(b) around $\eta^2 \sim 0.4$, while to our knowledge such a rigorous nonperturbative framework for studying cavity moiré materials with the continuum of quantized electromagnetic modes is currently lacking. Nevertheless, we argue that the effect we predict, the enhancement of magnetic frustration, is expected to be appreciable even in this regime. The reason for this is that the enhancement is based on a simple and general mechanism, namely, the emergence of long-range spin interactions mediated by the vacuum fluctuations of cavity fields; at this stage, we do not expect any particular reason for breakdown of

this mechanism in nonperturbative regions. In addition, it is also important to note that the essence of controlling magnetic phases of moiré materials is the band renormalization $\xi_{\mathbf{k}}$ in the effective Hamiltonian (10) which is larger than the original bare dispersion $\varepsilon_{\mathbf{k}}$ due to the band flatness. Therefore, the effect we predict becomes more appreciable in moiré materials with flatter electronic bands, and the transition might already take place in perturbative regimes. All in all, our findings would be of experimental relevance in view of recent developments in moiré materials and cavity QED, which demonstrates ultrasmall mode volumes of hyperbolic polaritons in nanosstructured materials [126–131].

Several open questions remain for future studies. In the present perturbation theory, we only retain the leading terms of $O(\eta^2)$, while the higher-order corrections might be important especially when $\eta = O(1)$. It would be interesting to analyze such a challenging regime on the basis of a nonperturbative approach allowing for nonvanishing electron-photon entanglement [135, 136]. It is also worthwhile to recall that the cavity-mediated hoppings $\eta^2 \tilde{\xi}_{ij}$ in Eq. (10) become more long-ranged as twist angle θ is increased. It merits further study to examine these large- θ regimes of cavity moiré materials beyond the parameter region considered here [137–139]; there, higher-order hoppings t_n should be increasingly important and an effective Hamiltonian may exhibit stronger magnetic frustration in which the ground-state phase diagram could be enriched. We hope that our work simulates further studies in these directions.

ACKNOWLEDGMENTS

We are grateful to Eugene Demler, Shunsuke Furukawa, Atac Imamoglu, Jun Mochida, Yao Wang, and Kenji Yasuda for fruitful discussions. K. M. acknowledges support from the Japan Society for the Promotion of Science (JSPS) through Grant No. JP24KJ0898. Y.A. acknowledges support from the Japan Society for the Promotion of Science (JSPS) through Grant No. JP19K23424 and from JST FOREST Program (Grant Number JPMJFR222U, Japan) and JST CREST (Grant Number JPMJCR23I2, Japan).

APPENDIX

Appendix A: Derivation of the effective Hamiltonian of the flat-band electrons

We here provide the detailed derivation of the effective Hamiltonian of flat-band electrons in Eq. (10) in the main text. Specifically, we start from the cavity moiré Hamiltonian in Eq. (3) in the main text. For the sake of generality, we consider the band structure shown in Fig. 6(a) as the dispersions $\varepsilon_{n\mathbf{k}}$ of the bare moiré Hamiltonian $\hat{H}_0 \equiv -\hat{\mathbf{p}}^2/2m^* + \Delta(\mathbf{r})$, where the flat band (la-

belled by $n = 0$) is located between the other electronic bands ($n \neq 0$). As described in the main text, the low-energy states of cavity moiré Hamiltonian (3) can be approximated by a product state $|\psi_e\rangle \otimes |0\rangle$, where $|0\rangle$ is the electromagnetic vacuum, and $|\psi_e\rangle$ is an electronic state with the partially-filled flat band and occupied (unoccupied) lower (upper) bands (cf. Fig. 6(b)). Accordingly, we define the projection operator \hat{P} onto the manifold spanned by these states and obtain the effective Hamiltonian in this subspace by employing the perturbation theory with respect to the (dimensionless) light-matter coupling strength $\eta = \sqrt{\sum_{\mathbf{q}} g_{\mathbf{q}}^2 / \omega_{\mathbf{q}}^2}$.

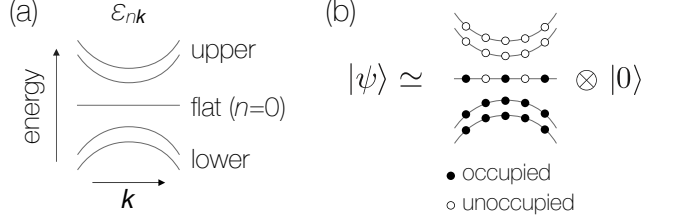


FIG. 6. (a) Schematic band dispersions of a moiré Hamiltonian $\hat{H}_0 = -\hat{\mathbf{p}}^2/2m^* + \Delta(\mathbf{r})$, where the flat band is located between the other electronic bands. (b) Approximate low-energy states $|\psi\rangle \simeq |\psi_e\rangle \otimes |0\rangle$ consisting of the product between the electromagnetic vacuum $|0\rangle$ and an electronic state $|\psi_e\rangle$ with the partially filled flat band and occupied (unoccupied) lower (upper) bands.

To proceed, we decompose the cavity moiré Hamiltonian (10) as

$$\hat{H} = \hat{H}_0 + \sum_{\mathbf{q}} \hbar \omega'_{\mathbf{q}} \hat{a}_{\mathbf{q}}^\dagger \hat{a}_{\mathbf{q}} + \hat{H}_I^{(p)} + \hat{H}_I^{(q)} + \hat{U}, \quad (\text{A1})$$

$$\omega'_{\mathbf{q}} = \omega_{\mathbf{q}} \left(1 - \frac{N_e e^2 A_{\mathbf{q}}^2}{m^* \hbar \omega_{\mathbf{q}}} \right) = \omega_{\mathbf{q}} \left(1 - \frac{N_e g_{\mathbf{q}}^2}{\omega_{\mathbf{q}}^2} \right), \quad (\text{A2})$$

$$\hat{H}_I^{(p)} = - \sum_{\mathbf{q}} \frac{e A_{\mathbf{q}}}{m^*} \left(\sum_{\sigma} \int d^2 \mathbf{r} \hat{\psi}_{\sigma \mathbf{r}}^\dagger \frac{(\hat{\mathbf{p}} \cdot \mathbf{e}_{\mathbf{q}}) e^{i \mathbf{q} \cdot \mathbf{r}} + e^{i \mathbf{q} \cdot \mathbf{r}} (\hat{\mathbf{p}} \cdot \mathbf{e}_{\mathbf{q}})}{2} \hat{\psi}_{\sigma \mathbf{r}} \right) \hat{a}_{\mathbf{q}} + \text{H.c.}, \quad (\text{A3})$$

$$\begin{aligned} \hat{H}_I^{(q)} &= \sum_{\mathbf{q}_1, \mathbf{q}_2} \sum_{\sigma} \int d^2 \mathbf{r} \hat{\psi}_{\sigma \mathbf{r}}^\dagger \frac{e^2 A_{\mathbf{q}_1} A_{\mathbf{q}_2}}{2m^*} \mathbf{e}_{\mathbf{q}_1} \cdot \mathbf{e}_{\mathbf{q}_2} (\hat{a}_{\mathbf{q}_1} \hat{a}_{\mathbf{q}_2} e^{i(\mathbf{q}_1 + \mathbf{q}_2) \cdot \mathbf{r}} + \text{H.c.}) \hat{\psi}_{\sigma \mathbf{r}} \\ &\quad + \sum_{\mathbf{q}_1 \neq \mathbf{q}_2} \sum_{\sigma} \int d^2 \mathbf{r} \hat{\psi}_{\sigma \mathbf{r}}^\dagger \frac{e^2 A_{\mathbf{q}_1} A_{\mathbf{q}_2}}{2m^*} \mathbf{e}_{\mathbf{q}_1} \cdot \mathbf{e}_{\mathbf{q}_2} (\hat{a}_{\mathbf{q}_1}^\dagger \hat{a}_{\mathbf{q}_2} e^{-i(\mathbf{q}_1 - \mathbf{q}_2) \cdot \mathbf{r}} + \text{H.c.}) \hat{\psi}_{\sigma \mathbf{r}}, \end{aligned} \quad (\text{A4})$$

where $\hat{H}_I^{(p)}$ is the paramagnetic term, and the A^2 diamagnetic term leads to the renormalized cavity frequency $\omega'_{\mathbf{q}}$ and the interaction term $\hat{H}_I^{(q)}$. In Eq. (A2), we define the total number of electrons by $N_e = \sum_{\sigma} \int d^2 \mathbf{r} \hat{\psi}_{\sigma \mathbf{r}}^\dagger \hat{\psi}_{\sigma \mathbf{r}}$, which is an order of V/v_M with the system size V and the volume of the moiré supercell v_M . Since the coupling strength $g_{\mathbf{q}}$ is proportional to $\sqrt{1/V}$, the frequency

renormalization in Eq. (A2) is $O(V^0 \eta^2)$. Below, we treat the first two terms in the right hand side of Eq. (A1) as the unperturbed Hamiltonian and incorporate the effect of $\hat{H}_I^{(p)} + \hat{H}_I^{(q)}$ by the perturbation theory.

Since $\hat{P} \hat{H}_I^{(p)} \hat{P} = \hat{P} \hat{H}_I^{(q)} \hat{P} = 0$, the leading terms come from the second-order perturbation of the paramagnetic term $\hat{H}_I^{(p)}$, which can be expressed in the Bloch basis as

$$\hat{H}_I^{(p)} = - \sum_{\mathbf{k}\sigma} \sum_{mn} \sum_{\mathbf{q}} \frac{e A_{\mathbf{q}}}{m^*} \mathbf{e}_{\mathbf{q}} \cdot \langle \psi_{m\mathbf{k}+\mathbf{q}\sigma} | \frac{\hat{\mathbf{p}} e^{i \mathbf{q} \cdot \mathbf{r}} + e^{i \mathbf{q} \cdot \mathbf{r}} \hat{\mathbf{p}}}{2} | \psi_{n\mathbf{k}\sigma} \rangle \hat{c}_{m\mathbf{k}+\mathbf{q}\sigma}^\dagger \hat{c}_{n\mathbf{k}\sigma} \hat{a}_{\mathbf{q}} + \text{H.c.} \quad (\text{A5})$$

$$= - \sum_{\mathbf{k}\sigma} \sum_{mn} \sum_{\mathbf{q}} \frac{e A_{\mathbf{q}}}{m^*} \mathbf{e}_{\mathbf{q}} \cdot \langle u_{m\mathbf{k}+\mathbf{q}} | \left(\hat{\mathbf{p}} + \hbar \left(\mathbf{k} + \frac{\mathbf{q}}{2} \right) \right) | u_{n\mathbf{k}} \rangle \hat{c}_{m\mathbf{k}+\mathbf{q}\sigma}^\dagger \hat{c}_{n\mathbf{k}\sigma} \hat{a}_{\mathbf{q}} + \text{H.c.} \quad (\text{A6})$$

$$= - \sum_{\mathbf{k}\sigma} \sum_{mn} \sum_{\mathbf{q}} \frac{e A_{\mathbf{q}}}{\hbar} (\mathbf{G}_{mn}^{\mathbf{k}, \mathbf{q}} \cdot \mathbf{e}_{\mathbf{q}}) \hat{c}_{m\mathbf{k}+\mathbf{q}\sigma}^\dagger \hat{c}_{n\mathbf{k}\sigma} \hat{a}_{\mathbf{q}} + \text{H.c.} \quad (\text{A7})$$

Here, we introduce the annihilation (creation) operator

$\hat{c}_{n\mathbf{k}\sigma}^{(\dagger)}$ corresponding to the Bloch state $|\psi_{n\mathbf{k}\sigma}\rangle$ with the

spin index σ and also define the multiband coefficients $\mathbf{G}_{mn}^{\mathbf{k},\mathbf{q}} \equiv \langle u_{m\mathbf{k}+\mathbf{q}} | \nabla_{\mathbf{k}} \hat{H}_{\mathbf{k}+\mathbf{q}/2} | u_{n\mathbf{k}} \rangle$, where $|u_{n\mathbf{k}}\rangle$ is related to $|\psi_{n\mathbf{k}\sigma}\rangle$ via $|\psi_{n\mathbf{k}\sigma}\rangle = e^{i\mathbf{k}\cdot\hat{\mathbf{r}}} |u_{n\mathbf{k}}\rangle \otimes |\sigma\rangle$ with spin state $|\sigma\rangle$. Figures 7(a)-(c) show the virtual processes relevant to

the second-order perturbation of $\hat{H}_I^{(p)}$, each of which corresponds to the virtual electronic transitions (a) within the flat band, (b) to the upper bands, and (c) from the lower bands, respectively. Approximating the excitation energy ΔE in each process as shown in Fig. 7, we get the following effective Hamiltonian of flat-band electrons:

$$\hat{H}_{\text{eff}} = \sum_{\mathbf{k}\sigma} \varepsilon_{0\mathbf{k}} \hat{c}_{\mathbf{k}\sigma}^\dagger \hat{c}_{\mathbf{k}\sigma} + \hat{H}_{\text{ff}} + \hat{H}_{\text{fu}} + \hat{H}_{\text{fl}} + \hat{U}, \quad (\text{A8})$$

$$\begin{aligned} \hat{H}_{\text{ff}} = & - \sum_{\mathbf{k}, \mathbf{k}'} \sum_{\sigma, \sigma'} \sum_{\mathbf{q}} \frac{m^*}{\hbar^2} \frac{g_{\mathbf{q}}^2}{\omega'_{\mathbf{q}}^2} (\mathbf{G}_{00}^{\mathbf{k}, \mathbf{q}} \cdot \mathbf{e}_{\mathbf{q}}) (\mathbf{G}_{00}^{\mathbf{k}', \mathbf{q}^*} \cdot \mathbf{e}_{\mathbf{q}}) \hat{c}_{\mathbf{k}+\mathbf{q}\sigma}^\dagger \hat{c}_{\mathbf{k}'-\mathbf{q}\sigma'}^\dagger \hat{c}_{\mathbf{k}'\sigma'} \hat{c}_{\mathbf{k}\sigma} \\ & - \sum_{\mathbf{k}\sigma} \frac{m^*}{\hbar^2} \left(\sum_{\mathbf{q}} \frac{g_{\mathbf{q}}^2}{\omega'_{\mathbf{q}}^2} |\mathbf{G}_{00}^{\mathbf{k}, \mathbf{q}} \cdot \mathbf{e}_{\mathbf{q}}|^2 \right) \hat{c}_{\mathbf{k}\sigma}^\dagger \hat{c}_{\mathbf{k}\sigma}, \end{aligned} \quad (\text{A9})$$

$$\hat{H}_{\text{fu}} = - \sum_{\mathbf{k}\sigma} \frac{m^*}{\hbar^2} \left(\sum_{\mathbf{q}} \sum_n^{\text{upper}} \frac{g_{\mathbf{q}}^2}{\omega'_{\mathbf{q}}^2} \frac{\hbar\omega'_{\mathbf{q}}}{\hbar\omega'_{\mathbf{q}} + \varepsilon_{n\mathbf{k}+\mathbf{q}} - \varepsilon_{0\mathbf{k}}} |\mathbf{G}_{n0}^{\mathbf{k}, \mathbf{q}} \cdot \mathbf{e}_{\mathbf{q}}|^2 \right) \hat{c}_{\mathbf{k}\sigma}^\dagger \hat{c}_{\mathbf{k}\sigma}, \quad (\text{A10})$$

$$\hat{H}_{\text{fl}} = \sum_{\mathbf{k}\sigma} \frac{m^*}{\hbar^2} \left(\sum_{\mathbf{q}} \sum_n^{\text{lower}} \frac{g_{\mathbf{q}}^2}{\omega'_{\mathbf{q}}^2} \frac{\hbar\omega'_{\mathbf{q}}}{\hbar\omega'_{\mathbf{q}} + \varepsilon_{0\mathbf{k}} - \varepsilon_{n\mathbf{k}+\mathbf{q}}} |\mathbf{G}_{0n}^{\mathbf{k}, \mathbf{q}} \cdot \mathbf{e}_{\mathbf{q}}|^2 \right) \hat{c}_{\mathbf{k}\sigma}^\dagger \hat{c}_{\mathbf{k}\sigma}, \quad (\text{A11})$$

where $\hat{c}_{\mathbf{k}\sigma}^{(\dagger)} = \hat{c}_{0\mathbf{k}\sigma}^{(\dagger)}$ is the annihilation (creation) operator of the flat-band electrons, and $\sum_n^{\text{upper(lower)}}$ denotes the

summation over the upper (lower) bands. In deriving Eqs. (A9)-(A11), we assume the relations $g_{\mathbf{q}} = g_{-\mathbf{q}}$ and $\omega'_{\mathbf{q}} = \omega'_{-\mathbf{q}}$ that hold true for uniaxial cavities, and use the following equalities:

$$\hat{P}(\hat{c}_{0\mathbf{k}\sigma}^\dagger \hat{c}_{n\mathbf{k}+\mathbf{q}\sigma} \hat{c}_{n'\mathbf{k}'+\mathbf{q}\sigma'}^\dagger \hat{c}_{0\mathbf{k}'\sigma'}) \hat{P} = \delta_{nn'} \delta_{\mathbf{k}\mathbf{k}'} \delta_{\sigma\sigma'} \hat{c}_{0\mathbf{k}\sigma}^\dagger \hat{c}_{0\mathbf{k}\sigma} \quad (n, n' : \text{upper bands}), \quad (\text{A12})$$

$$\hat{P}(\hat{c}_{n\mathbf{k}+\mathbf{q}\sigma}^\dagger \hat{c}_{0\mathbf{k}\sigma} \hat{c}_{0\mathbf{k}'\sigma'}^\dagger \hat{c}_{n'\mathbf{k}'+\mathbf{q}\sigma'}) \hat{P} = \delta_{nn'} \delta_{\mathbf{k}\mathbf{k}'} \delta_{\sigma\sigma'} \hat{c}_{0\mathbf{k}\sigma}^\dagger \hat{c}_{0\mathbf{k}\sigma} \quad (n, n' : \text{lower bands}). \quad (\text{A13})$$

We note that the first term in the right hand side of Eq. (A9) is the Amperean electron-electron interaction mediated by cavity electromagnetic fields [98]. Since the coefficients $(\mathbf{G}_{00}^{\mathbf{k}, \mathbf{q}} \cdot \mathbf{e}_{\mathbf{q}})(\mathbf{G}_{00}^{\mathbf{k}', \mathbf{q}^*} \cdot \mathbf{e}_{\mathbf{q}}) \approx (\nabla_{\mathbf{k}} \varepsilon_{0\mathbf{k}} \cdot \mathbf{e}_{\mathbf{q}})(\nabla_{\mathbf{k}} \varepsilon_{0\mathbf{k}'} \cdot \mathbf{e}_{\mathbf{q}})$ in this term almost vanish due to the band flatness, the Amperean interaction is negligibly small compared to the

Coulomb interaction \hat{U} . Retaining up to $O(\eta^2)$ -terms and taking the limit $\mathbf{q} \rightarrow \mathbf{0}$ in Eq. (A8) (which does not affect the results provided in the present work as detailed in Appendix B), we finally obtain the effective Hamiltonian of flat-band electrons as

$$\hat{H}_{\text{eff}} = \sum_{\mathbf{k}\sigma} (\varepsilon_{0\mathbf{k}} + \eta^2 \xi_{\mathbf{k}}) \hat{c}_{\mathbf{k}\sigma}^\dagger \hat{c}_{\mathbf{k}\sigma} + \hat{U}, \quad (\text{A14})$$

$$\xi_{\mathbf{k}} = \frac{m^*}{2\hbar^2} \left(-|\mathbf{G}_{00}^{\mathbf{k}}| - \sum_n^{\text{upper}} \frac{\hbar\omega_0}{\hbar\omega_0 + \varepsilon_{n\mathbf{k}} - \varepsilon_{0\mathbf{k}}} |\mathbf{G}_{n0}^{\mathbf{k}}|^2 + \sum_n^{\text{lower}} \frac{\hbar\omega_0}{\hbar\omega_0 + \varepsilon_{0\mathbf{k}} - \varepsilon_{n\mathbf{k}}} |\mathbf{G}_{0n}^{\mathbf{k}}|^2 \right), \quad (\text{A15})$$

where we introduce $\mathbf{G}_{mn}^{\mathbf{k}} \equiv \mathbf{G}_{mn}^{\mathbf{k}, \mathbf{0}}$ and use the fact that $\omega'_{\mathbf{q}}/\omega_{\mathbf{q}} = 1 + O(\eta^2)$. Since there are no upper bands

in the setup of the TMD heterobilayer considered in the main text, the effective Hamiltonian (A14) simplifies to Eq. (10) in the main text. We note that the effective Hamiltonian derived above is qualitatively different from the one obtained by using the single-mode approximation. In the latter case, the single-mode coupling $g/\omega = O(V^0)$ would be required to achieve the ultrastrong coupling $g^2/\omega^2 = O(1)$, and thus, the renormalization of the cavity frequency due to A^2 diamagnetic term should be $O(V^1)$. Also, we note that possible modification of the Coulomb interaction U , which is at most $O(\eta^2)$, is not included since it does not affect the discussions in the present work as detailed in Appendix C.

Making appropriate modifications in the moiré Hamiltonian (1), our procedure can also be applied to other moiré materials, such as a TMD moiré homobilayer or a twisted bilayer graphene. In a TMD moiré homobilayer, the moiré Hamiltonian of spin-up electrons (or equivalently, K-valley electrons in the TMD monolayers) is given as [3, 31],

$$\hat{H}_{0\uparrow} = \begin{pmatrix} -\frac{(\hat{\mathbf{p}} - \hbar\boldsymbol{\kappa}_b)^2}{2m^*} & \\ & -\frac{(\hat{\mathbf{p}} - \hbar\boldsymbol{\kappa}_t)^2}{2m^*} \end{pmatrix} + \hat{\Delta}(\mathbf{r}), \quad (\text{A16})$$

where the 2×2 -matrix corresponds to the two layer degrees of freedom, and $\hat{\Delta}(\mathbf{r})$ is a 2×2 -matrix-valued moiré potential. Here, $\boldsymbol{\kappa}_{t(b)}$ denotes the distinct mBZ corner, which originates from the K-valley of the top (bottom) TMD monolayer (cf. Fig. 8). The moiré

Hamiltonian of spin-down electrons $\hat{H}_{0\downarrow}$ is given as the time-reversal (TR) pair of $\hat{H}_{0\uparrow}$. We note that $\hat{H}_{0\uparrow(\downarrow)}$ does not have TR-symmetry $(\hat{\mathbf{p}}, \hat{\Delta}(\mathbf{r})) \rightarrow (-\hat{\mathbf{p}}, \hat{\Delta}^*(\mathbf{r}))$, while the total moiré Hamiltonian $\hat{H}_{0\uparrow} + \hat{H}_{0\downarrow}$ does $(\hat{\mathbf{p}}, \hat{\Delta}(\mathbf{r}), \sigma) \rightarrow (-\hat{\mathbf{p}}, \hat{\Delta}^*(\mathbf{r}), -\sigma)$. As a result, the hopping amplitudes $t_{ij,\sigma}$ in the tight-binding description are in general complex-valued and satisfy $t_{ij,-\sigma} = t_{ij,\sigma}^*$. Similarly, in a twisted bilayer graphene, the moiré Hamiltonian of spin-up and K-valley electrons is given as [2, 3],

$$\hat{H}_{0\uparrow\text{K}} = \begin{pmatrix} v_F(\hat{\mathbf{p}} - \hbar\boldsymbol{\kappa}_b) \cdot \hat{\boldsymbol{\sigma}} & \\ & v_F(\hat{\mathbf{p}} - \hbar\boldsymbol{\kappa}_t) \cdot \hat{\boldsymbol{\sigma}} \end{pmatrix} + \hat{\Delta}(\mathbf{r}), \quad (\text{A17})$$

where v_F is the Fermi velocity of monolayer graphene, $\hat{\boldsymbol{\sigma}} = (\hat{\sigma}_x, \hat{\sigma}_y)^T$, and $\hat{\Delta}(\mathbf{r})$ is a 4×4 -matrix-valued moiré potential corresponding to the layer and sublattice degrees of freedom.

Appendix B: On the validity of the approximation made when deriving effective Hamiltonian of flat-band electrons

In the last step of the above derivation described in Appendix A, we neglect the \mathbf{q} -dependences of $\mathbf{G}_{0n}^{k,q}$ and $\hbar\omega_q / (\hbar\omega_q + \varepsilon_{0k} - \varepsilon_{nk+q})$ in Eqs. (A9)-(A11) and approximate them as

$$\hat{H}_{\text{fu}} = \sum_{\mathbf{k}\sigma} \frac{m^*}{\hbar^2} \left(\sum_{\mathbf{q}} \sum_n^{\text{lower}} \frac{g_{\mathbf{q}}^2}{\omega_{\mathbf{q}}^2} \frac{\hbar\omega_{\mathbf{q}}}{\hbar\omega_{\mathbf{q}} + \varepsilon_{0k} - \varepsilon_{nk+q}} |\mathbf{G}_{0n}^{k,q} \cdot \mathbf{e}_q|^2 \right) \hat{c}_{\mathbf{k}\sigma}^\dagger \hat{c}_{\mathbf{k}\sigma} + O(\eta^4) \quad (\text{B1})$$

$$\simeq \sum_{\mathbf{k}\sigma} \frac{m^*}{\hbar^2} \left(\sum_{\mathbf{q}} \frac{g_{\mathbf{q}}^2}{\omega_{\mathbf{q}}^2} \sum_n^{\text{lower}} \frac{\hbar\omega_0}{\hbar\omega_0 + \varepsilon_{0k} - \varepsilon_{nk}} |\mathbf{G}_{0n}^{k,0} \cdot \mathbf{e}_q|^2 \right) \hat{c}_{\mathbf{k}\sigma}^\dagger \hat{c}_{\mathbf{k}\sigma}. \quad (\text{B2})$$

To demonstrate the validity of this approximation, we compare the main results in the main text obtained with or without making such approximation. Below, to include the effect of momentum dependence of the coupling strengths $g_{\mathbf{q}}/\omega_{\mathbf{q}}$, we assume that $g_{\mathbf{q}}^2/\omega_{\mathbf{q}}^2$ can be approximated by a simple Gaussian function as

$$\frac{g_{\mathbf{q}}^2}{\omega_{\mathbf{q}}^2} = \frac{\eta^2}{\mathcal{N}} \exp\left(-\frac{\mathbf{q}^2}{2q_c^2}\right), \quad (\text{B3})$$

where \mathcal{N} is determined by the normalization condition $\sum_{\mathbf{q}} g_{\mathbf{q}}^2/\omega_{\mathbf{q}}^2 = \eta^2$. Also, we shall define the effective width Q of the coupling strength by the condition $\sum_{|\mathbf{q}| < Q} g_{\mathbf{q}}^2/\omega_{\mathbf{q}}^2 = 0.95\eta^2 \Leftrightarrow Q/q_c = \sqrt{-2 \ln 0.05}$.

Figure 9 shows the ground-state phase diagrams of the cavity-confined TMD heterobilayer obtained with or without making the above approximation. At finite Q ,

we can see that $\xi_{\mathbf{k}}$ is slightly modified and the highly frustrated phases such as the zigzag phase become bit narrower accordingly. These modifications are consistent with the expectation that the cavity-mediated long-range hoppings now have an effective cutoff length scale $\sim 1/Q$. Nevertheless, as inferred from the figure, these changes are almost negligible, and it is clear that all the results remain qualitatively the same, which justifies the validity of our treatment.

Appendix C: Effect of the modification of the Coulomb interaction

We here discuss possible modification of the Coulomb interaction due to the cavity confinement. We recall

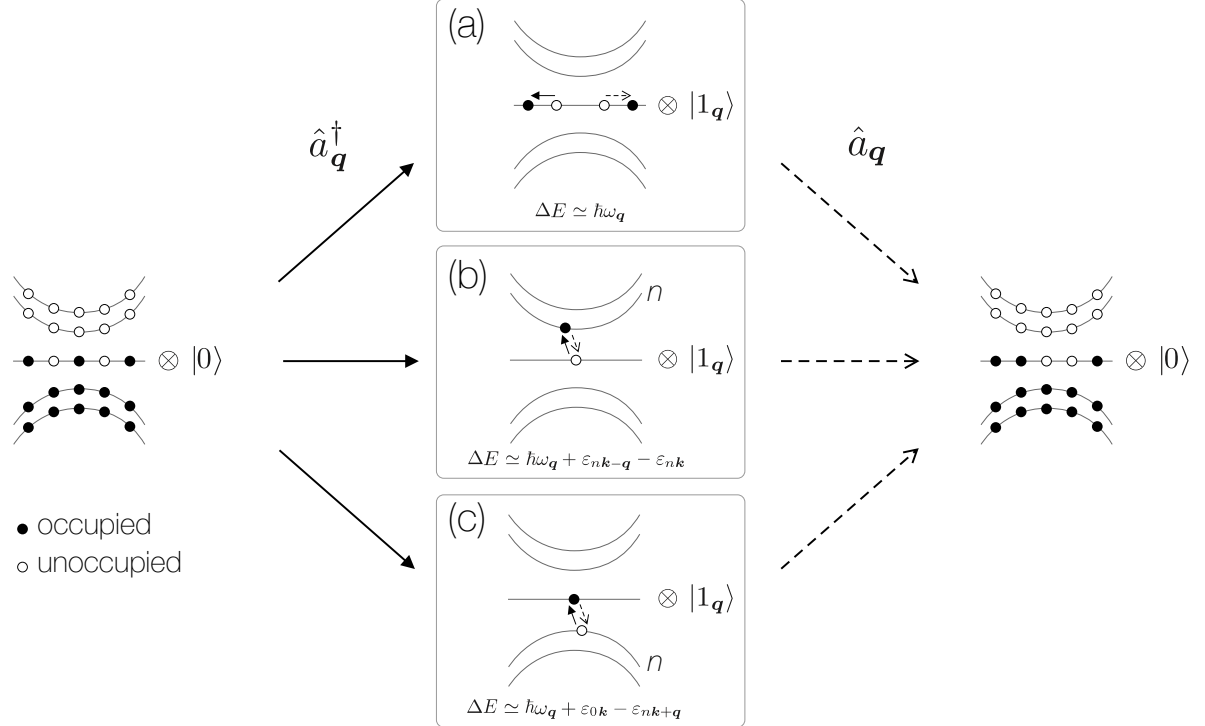


FIG. 7. Virtual processes in the second-order perturbation of the paramagnetic term $\hat{H}_I^{(p)}$, where a cavity mode is excited by \hat{a}_q^\dagger with (a) intraband transitions within the flat band, (b) interband transitions from the flat band to an upper band, and (c) interband transitions from a lower band to the flat band. We approximate excitation energies in each process ΔE as shown in (a)-(c).

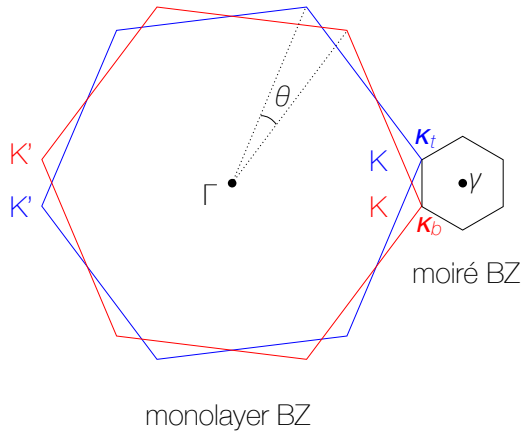


FIG. 8. Moiré Brillouin Zone (mBZ) for spin-up (K-valley) electrons of TMD moiré homobilayer with twist angle θ . We also show the monolayer BZ of the top (blue) and bottom (red) TMD layers.

that, in the present analysis, the only assumption on the Coulomb interaction is that the interaction strength U is much larger than the hopping amplitudes of tight-binding

orbitals of flat-band electrons t_i . This assumption generally holds true in moiré materials due to the band flatness. In particular, the ratio between the magnetic interactions J_i , which determines the magnetic phases of the moiré bilayer, is independent of the Coulomb interaction strength U in the present analysis. Since possible modification of the Coulomb interaction is at most an order of $O(\eta^2)$ compared to the original value as detailed below, we conclude that it does not affect the discussions in the present work.

In moiré materials, one can estimate the strength of the Coulomb interaction U by the matrix element

$$U \equiv \langle w_0 | \hat{U} | w_0 \rangle = \int d\mathbf{r} \int d\mathbf{r}' U(\mathbf{r} - \mathbf{r}') w_0^*(\mathbf{r}) w_0(\mathbf{r}'), \quad (C1)$$

where $|w_0\rangle$ is the Wannier orbital constructed from the Bloch states of the moiré flat band, and $U(\mathbf{r}) = (e^2/\epsilon)[r^{-1} - (r^2 + D^2)^{-1/2}]$ is the screened Coulomb potential in moiré materials [137]. In the present setup of cavity moiré materials, the modification of the Coulomb interaction originates from the modification of the Bloch states $|\psi_{0\mathbf{k}}\rangle$ due to the interaction with hyperbolic cavities. Within the perturbation theory, the Bloch states are modified as

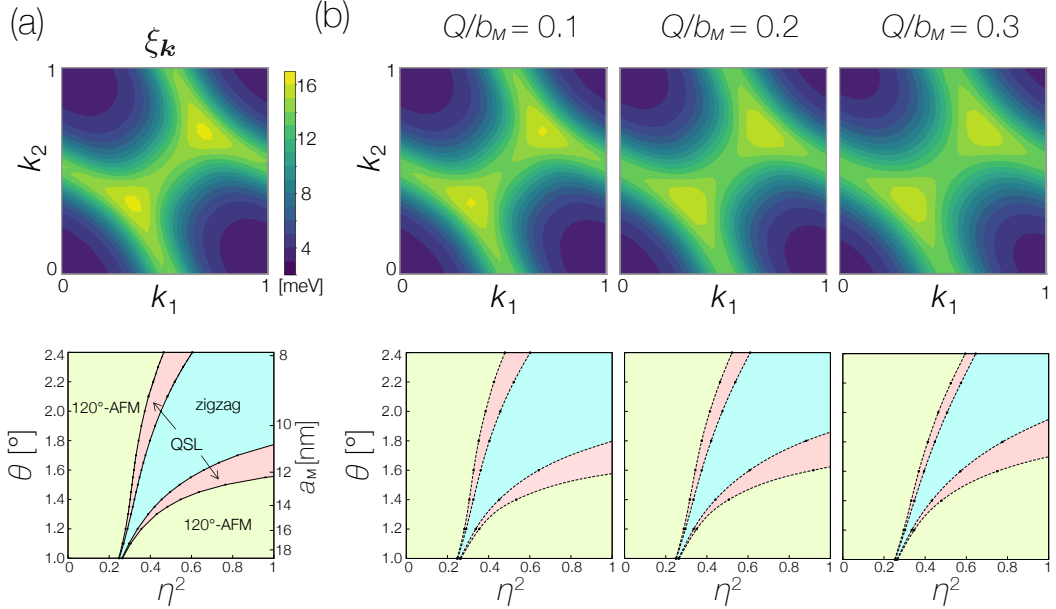


FIG. 9. (a) Cavity dressing $\xi_{\mathbf{k}}$ (top panel) and the ground-state phase diagram of the cavity-confined TMD heterobilayer (bottom panel) obtained with the approximation (B2). We define k_1 and k_2 via $\mathbf{k} = k_1 \mathbf{b}_1 + k_2 \mathbf{b}_2$. (b) Cavity dressing $\xi_{\mathbf{k}}$ (top panels) and ground-state phase diagrams (bottom panels) obtained without the approximation. Here, Q is the effective width of the coupling strength (B3), and $b_M = 4\pi/(\sqrt{3}a_M)$ is the size of the moiré Brillouin zone.

$$|\psi_{0\mathbf{k}}\rangle \rightarrow |\psi'_{0\mathbf{k}}\rangle = |\psi_{0\mathbf{k}}\rangle |0\rangle + \sum_{n \neq 0} \sum_{\mathbf{q}} \frac{1}{\hbar\omega_{\mathbf{q}} + \varepsilon_{0\mathbf{k}} - \varepsilon_{n\mathbf{k}-\mathbf{q}}} \frac{eA_{\mathbf{q}}}{\hbar} (\mathbf{G}_{0n}^{\mathbf{k}-\mathbf{q},\mathbf{q}} \cdot \mathbf{e}_{\mathbf{q}})^* |\psi_{n\mathbf{k}-\mathbf{q}}\rangle |1_{\mathbf{q}}\rangle + O(\eta^2), \quad (\text{C2})$$

where $|0\rangle$ is the cavity vacuum, and $|1_{\mathbf{q}}\rangle = \hat{a}_{\mathbf{q}}^\dagger |0\rangle$ is the one-phonon-polariton excited state with in-plane momentum \mathbf{q} . Thus, the Wannier orbital, the superposition of the Bloch states, is modified as

$$|w_0\rangle \rightarrow |w'_0\rangle = |w_0\rangle |0\rangle + \sum_{\mathbf{q}} |w_{\mathbf{q}}^{(1)}\rangle |1_{\mathbf{q}}\rangle + O(\eta^2), \quad (\text{C3})$$

$$|w_{\mathbf{q}}^{(1)}\rangle = \int \frac{v_M d^2\mathbf{k}}{(2\pi)^2} \sum_{n \neq 0} \frac{1}{\hbar\omega_{\mathbf{q}} + \varepsilon_{0\mathbf{k}} - \varepsilon_{n\mathbf{k}-\mathbf{q}}} \frac{eA_{\mathbf{q}}}{\hbar} (\mathbf{G}_{0n}^{\mathbf{k}-\mathbf{q},\mathbf{q}} \cdot \mathbf{e}_{\mathbf{q}})^* |\psi_{n\mathbf{k}-\mathbf{q}}\rangle, \quad (\text{C4})$$

where we note that $|w_{\mathbf{q}}^{(1)}\rangle$ is $O(\eta)$. Since the second term in the right hand side of Eq. (C3) includes the cavity excited state $|1_{\mathbf{q}}\rangle$, the modification of the Coulomb interaction becomes $O(U \cdot \eta^2)$ as

$$U \rightarrow U' = \frac{\langle w'_0 | \hat{U} | w'_0 \rangle}{\langle w'_0 | w'_0 \rangle} = \frac{\langle w_0 | \hat{U} | w_0 \rangle + \sum_{\mathbf{q}} \langle w_{\mathbf{q}}^{(1)} | \hat{U} | w_{\mathbf{q}}^{(1)} \rangle + O(U \cdot \eta^2)}{\langle w_0 | w_0 \rangle + \sum_{\mathbf{q}} \langle w_{\mathbf{q}}^{(1)} | w_{\mathbf{q}}^{(1)} \rangle + O(\eta^2)} = \langle w_0 | \hat{U} | w_0 \rangle + O(U \cdot \eta^2), \quad (\text{C5})$$

which proves the statement above.

Appendix D: Effect of the polariton loss in the hyperbolic cavity

We here discuss a possible effect of loss of the phonon polaritons in the hyperbolic cavity. In general, the loss rate of hyperbolic polaritons is very low compared to the optical phonon frequency in vdW crystals $\hbar\omega_{\mathbf{q}} = 10^2 \sim$

10^3 meV. To estimate the strength of the polariton loss, we first recall that the frequency $\omega_{\mathbf{q}}$ (and out-of-plane momentum $\kappa_{\mathbf{q}}$) of the polariton mode with in-plane momentum \mathbf{q} is determined by the eigenequations of elec-

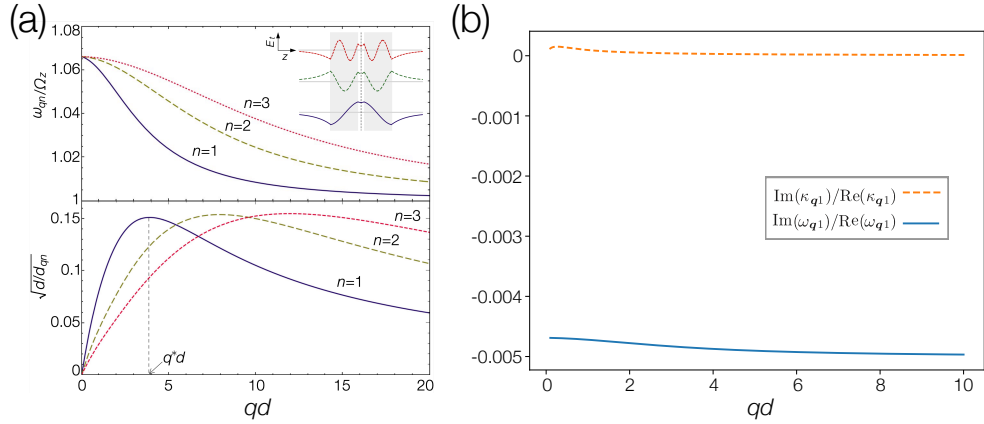


FIG. 10. (a) Dispersions ω_{qn} of the hyperbolic phonon polaritons (top panel) and inverse of the square root of the dimensionless effective confinement length d_{qn}/d , which is proportional to the coupling strength g_q/ω_q . Reproduced from Fig. 2 in Ref. [115]. (b) The ratio between the imaginary part and the real part of the out-of-plane momenta κ_q and the phonon-polariton frequencies ω_q . We plot the ratio for the $n = 1$ eigenmodes (see top panel in (a)). The parameters are the same as in Ref. [115], and we set the loss ratio as $\gamma_z/\Omega_z = \gamma_t/\Omega_t = 0.01$.

tromagnetic fields as [115]

$$\frac{\mathbf{q}^2}{\epsilon_z(\omega)} + \frac{\kappa^2}{\epsilon_t(\omega)} = \frac{\omega^2}{\epsilon_0 c^2}, \quad (\text{D1})$$

$$\tan\left(\frac{\kappa d}{2}\right) = -\frac{\kappa}{-\epsilon_t(\omega)\sqrt{q^2 - \frac{\omega^2}{c^2}}}. \quad (\text{D2})$$

Here, $\epsilon_{t(z)}(\omega)$ is the in-plane (out-of-plane) permittivity of the dielectric medium, and d is the thickness of the vdW slabs. To include the effect of phonon loss in vdW materials, we can use the complex-valued permittivities as [130]

$$\epsilon_z(\omega) = \epsilon_{z\infty} \left(1 + \frac{\eta_z^2}{\Omega_z^2 - \omega^2 - i\gamma_z\omega}\right), \quad (\text{D3})$$

$$\epsilon_t(\omega) = \epsilon_{t\infty} \left(1 + \frac{\eta_t^2}{\Omega_t^2 - \omega^2 - i\gamma_t\omega}\right). \quad (\text{D4})$$

We note that an ultralow-loss ratio $\gamma/\Omega \sim 0.005$ has been achieved in hyperbolic vdW materials, such as hBN [130].

As \mathbf{q} is a real-valued variable corresponding to the in-plane momentum between the airgap of the cavity, the out-of-plane momentum κ and the cavity frequency ω in the solutions of the eigenequation are complex-valued, reflecting the phonon loss in the dielectric medium.

Figure 10 shows the ratio between the imaginary part and the real part of κ_q and ω_q , which are obtained by solving the eigenequations (D1), (D2) up to the first order of γ . The changes of κ_q and ω_q could in principle affect the value of the coupling strength; for instance, the change of κ_q modifies the spatial profile of each eigenmode and its mode amplitude. However, from the results we have obtained, we estimate the amount of the change in the coupling strength to be $\sim 0.5\%$, which only leads to the negligibly small shifts of the proposed phase boundaries. We thus expect that the polariton loss does not play an important role in our consideration based on the setup consisting of hyperbolic cavity with ultralow phonon losses.

-
- [1] J. M. B. Lopes dos Santos, N. M. R. Peres, and A. H. Castro Neto, *Phys. Rev. Lett.* **99**, 256802 (2007).
- [2] R. Bistritzer and A. H. MacDonald, *PNAS* **108**, 12233 (2011).
- [3] S. Carr, S. Fang, and E. Kaxiras, *Nat. Rev. Mater.* **5**, 748 (2020).
- [4] M. Koshino, N. F. Q. Yuan, T. Koretsune, M. Ochi, K. Kuroki, and L. Fu, *Phys. Rev. X* **8**, 031087 (2018).
- [5] H. C. Po, L. Zou, A. Vishwanath, and T. Senthil, *Phys. Rev. X* **8**, 031089 (2018).
- [6] E. Y. Andrei and A. H. MacDonald, *Nat. Mater.* **19**, 1265 (2020).
- [7] L. Balents, C. R. Dean, D. K. Efetov, and A. F. Young, *Nat. Phys.* **16**, 725 (2020).
- [8] K. P. Nuckolls, M. Oh, D. Wong, B. Lian, K. Watanabe, T. Taniguchi, B. A. Bernevig, and A. Yazdani, *Nature* **588**, 610 (2020).
- [9] Y. Cao, V. Fatemi, A. Demir, S. Fang, S. L. Tomarken,

- J. Y. Luo, J. D. Sanchez-Yamagishi, K. Watanabe, T. Taniguchi, E. Kaxiras, R. C. Ashoori, and P. Jarillo-Herrero, *Nature* **556**, 80 (2018).
- [10] G. W. Burg, J. Zhu, T. Taniguchi, K. Watanabe, A. H. MacDonald, and E. Tutuc, *Phys. Rev. Lett.* **123**, 197702 (2019).
- [11] G. Chen, L. Jiang, S. Wu, B. Lyu, H. Li, B. L. Chittari, K. Watanabe, T. Taniguchi, Z. Shi, J. Jung, Y. Zhang, and F. Wang, *Nat. Phys.* **15**, 237 (2019).
- [12] Y. Cao, V. Fatemi, S. Fang, K. Watanabe, T. Taniguchi, E. Kaxiras, and P. Jarillo-Herrero, *Nature* **556**, 43 (2018).
- [13] G. Chen, A. L. Sharpe, P. Gallagher, I. T. Rosen, E. J. Fox, L. Jiang, B. Lyu, H. Li, K. Watanabe, T. Taniguchi, J. Jung, Z. Shi, D. Goldhaber-Gordon, Y. Zhang, and F. Wang, *Nature* **572**, 215 (2019).
- [14] E. Codecido, Q. Wang, R. Koester, S. Che, H. Tian, R. Lv, S. Tran, K. Watanabe, T. Taniguchi, F. Zhang, M. Bockrath, and C. N. Lau, *Sci. Adv.* **5**, eaaw9770 (2019).
- [15] X. Lu, P. Stepanov, W. Yang, M. Xie, M. A. Aamir, I. Das, C. Urgell, K. Watanabe, T. Taniguchi, G. Zhang, A. Bachtold, A. H. MacDonald, and D. K. Efetov, *Nature* **574**, 653 (2019).
- [16] M. Yankowitz, S. Chen, H. Polshyn, Y. Zhang, K. Watanabe, T. Taniguchi, D. Graf, A. F. Young, and C. R. Dean, *Science* **363**, 1059 (2019).
- [17] A. L. Sharpe, E. J. Fox, A. W. Barnard, J. Finney, K. Watanabe, T. Taniguchi, M. A. Kastner, and D. Goldhaber-Gordon, *Science* **365**, 605 (2019).
- [18] G. Chen, A. L. Sharpe, E. J. Fox, Y.-H. Zhang, S. Wang, L. Jiang, B. Lyu, H. Li, K. Watanabe, T. Taniguchi, Z. Shi, T. Senthil, D. Goldhaber-Gordon, Y. Zhang, and F. Wang, *Nature* **579**, 56 (2020).
- [19] X. Liu, Z. Hao, E. Khalaf, J. Y. Lee, Y. Ronen, H. Yoo, D. Haei Najafabadi, K. Watanabe, T. Taniguchi, A. Vishwanath, and P. Kim, *Nature* **583**, 221 (2020).
- [20] M. He, Y.-H. Zhang, Y. Li, Z. Fei, K. Watanabe, T. Taniguchi, X. Xu, and M. Yankowitz, *Nat. Commun.* **12**, 4727 (2021).
- [21] C. R. Dean, L. Wang, P. Maher, C. Forsythe, F. Ghahari, Y. Gao, J. Katoch, M. Ishigami, P. Moon, M. Koshino, T. Taniguchi, K. Watanabe, K. L. Shepard, J. Hone, and P. Kim, *Nature* **497**, 598 (2013).
- [22] B. Hunt, J. D. Sanchez-Yamagishi, A. F. Young, M. Yankowitz, B. J. LeRoy, K. Watanabe, T. Taniguchi, P. Moon, M. Koshino, P. Jarillo-Herrero, and R. C. Ashoori, *Science* **340**, 1427 (2013).
- [23] L. Wang, Y. Gao, B. Wen, Z. Han, T. Taniguchi, K. Watanabe, M. Koshino, J. Hone, and C. R. Dean, *Science* **350**, 1231 (2015).
- [24] E. M. Spanton, A. A. Zibrov, H. Zhou, T. Taniguchi, K. Watanabe, M. P. Zaletel, and A. F. Young, *Science* **360**, 62 (2018).
- [25] Y. Liu, Y. Huang, and X. Duan, *Nature* **567**, 323 (2019).
- [26] T. Vincent, J. Liang, S. Singh, E. G. Castanon, X. Zhang, A. McCreary, D. Jariwala, O. Kazakova, and Z. Y. Al Balushi, *Appl. Phys. Rev.* **8**, 041320 (2021).
- [27] D. M. Kennes, M. Claassen, L. Xian, A. Georges, A. J. Millis, J. Hone, C. R. Dean, D. N. Basov, A. N. Pasupathy, and A. Rubio, *Nat. Phys.* **17**, 155 (2021).
- [28] F. Wu, T. Lovorn, E. Tutuc, and A. H. MacDonald, *Phys. Rev. Lett.* **121**, 026402 (2018).
- [29] L. Classen, C. Honerkamp, and M. M. Scherer, *Phys. Rev. B* **99**, 195120 (2019).
- [30] L. Xian, D. M. Kennes, N. Tancogne-Dejean, M. Altarelli, and A. Rubio, *Nano Lett.* **19**, 4934 (2019).
- [31] F. Wu, T. Lovorn, E. Tutuc, I. Martin, and A. H. MacDonald, *Phys. Rev. Lett.* **122**, 086402 (2019).
- [32] H. Pan, F. Wu, and S. Das Sarma, *Phys. Rev. Res.* **2**, 033087 (2020).
- [33] H. Pan, F. Wu, and S. Das Sarma, *Phys. Rev. B* **102**, 201104 (2020).
- [34] M. Angeli and A. H. MacDonald, *PNAS* **118**, e2021826118 (2021).
- [35] N. C. Hu and A. H. MacDonald, *Phys. Rev. B* **104**, 214403 (2021).
- [36] N. Morales-Durán, A. H. MacDonald, and P. Potasz, *Phys. Rev. B* **103**, L241110 (2021).
- [37] J. Zang, J. Wang, J. Cano, and A. J. Millis, *Phys. Rev. B* **104**, 075150 (2021).
- [38] L. Xian, M. Claassen, D. Kiese, M. M. Scherer, S. Trebst, D. M. Kennes, and A. Rubio, *Nat. Commun.* **12**, 5644 (2021).
- [39] J. Zang, J. Wang, J. Cano, A. Georges, and A. J. Millis, *Phys. Rev. X* **12**, 021064 (2022).
- [40] C. Jin, E. C. Regan, A. Yan, M. Iqbal Bakti Utama, D. Wang, S. Zhao, Y. Qin, S. Yang, Z. Zheng, S. Shi, K. Watanabe, T. Taniguchi, S. Tongay, A. Zettl, and F. Wang, *Nature* **567**, 76 (2019).
- [41] G. X. Ni, H. Wang, B.-Y. Jiang, L. X. Chen, Y. Du, Z. Y. Sun, M. D. Goldflam, A. J. Frenzel, X. M. Xie, M. M. Fogler, and D. N. Basov, *Nat. Commun.* **10**, 4360 (2019).
- [42] E. C. Regan, D. Wang, C. Jin, M. I. Bakti Utama, B. Gao, X. Wei, S. Zhao, W. Zhao, Z. Zhang, K. Yumigeta, M. Blei, J. D. Carlström, K. Watanabe, T. Taniguchi, S. Tongay, M. Crommie, A. Zettl, and F. Wang, *Nature* **579**, 359 (2020).
- [43] Y. Shimazaki, I. Schwartz, K. Watanabe, T. Taniguchi, M. Kroner, and A. Imamoğlu, *Nature* **580**, 472 (2020).
- [44] Y. Tang, L. Li, T. Li, Y. Xu, S. Liu, K. Barmak, K. Watanabe, T. Taniguchi, A. H. MacDonald, J. Shan, and K. F. Mak, *Nature* **579**, 353 (2020).
- [45] L. Wang, E.-M. Shih, A. Ghiotto, L. Xian, D. A. Rhodes, C. Tan, M. Claassen, D. M. Kennes, Y. Bai, B. Kim, K. Watanabe, T. Taniguchi, X. Zhu, J. Hone, A. Rubio, A. N. Pasupathy, and C. R. Dean, *Nat. Mater.* **19**, 861 (2020).
- [46] Y. Xu, S. Liu, D. A. Rhodes, K. Watanabe, T. Taniguchi, J. Hone, V. Elser, K. F. Mak, and J. Shan, *Nature* **587**, 214 (2020).
- [47] Z. Zhang, Y. Wang, K. Watanabe, T. Taniguchi, K. Ueno, E. Tutuc, and B. J. LeRoy, *Nat. Phys.* **16**, 1093 (2020).
- [48] X. Huang, T. Wang, S. Miao, C. Wang, Z. Li, Z. Lian, T. Taniguchi, K. Watanabe, S. Okamoto, D. Xiao, S.-F. Shi, and Y.-T. Cui, *Nat. Phys.* **17**, 715 (2021).
- [49] C. Jin, Z. Tao, T. Li, Y. Xu, Y. Tang, J. Zhu, S. Liu, K. Watanabe, T. Taniguchi, J. C. Hone, L. Fu, J. Shan, and K. F. Mak, *Nat. Mater.* **20**, 940 (2021).
- [50] K. Yasuda, X. Wang, K. Watanabe, T. Taniguchi, and P. Jarillo-Herrero, *Science* **372**, 1458 (2021).
- [51] T. Li, S. Jiang, L. Li, Y. Zhang, K. Kang, J. Zhu, K. Watanabe, T. Taniguchi, D. Chowdhury, L. Fu, J. Shan, and K. F. Mak, *Nature* **597**, 350 (2021).
- [52] L. Savary and L. Balents, *Rep. Prog. Phys.* **80**, 016502

- (2016).
- [53] Y. Zhou, K. Kanoda, and T.-K. Ng, *Rev. Mod. Phys.* **89**, 025003 (2017).
- [54] M.-H. Zare and H. Mosadeq, *Phys. Rev. B* **104**, 115154 (2021).
- [55] D. Kiese, Y. He, C. Hickey, A. Rubio, and D. M. Kennes, *APL Mater.* **10**, 031113 (2022).
- [56] A. A. Anappara, S. De Liberato, A. Tredicucci, C. Ciuti, G. Biasiol, L. Sorba, and F. Beltram, *Phys. Rev. B* **79**, 201303 (2009).
- [57] G. Scalari, C. Maissen, D. Turčinková, D. Hagenmüller, S. De Liberato, C. Ciuti, C. Reichl, D. Schuh, W. Wegscheider, M. Beck, and J. Faist, *Science* **335**, 1323 (2012).
- [58] G. Scalari, C. Maissen, S. Cibella, R. Leoni, P. Carelli, F. Valmorra, M. Beck, and J. Faist, *New J. Phys.* **16**, 033005 (2014).
- [59] C. Maissen, G. Scalari, F. Valmorra, M. Beck, J. Faist, S. Cibella, R. Leoni, C. Reichl, C. Charpentier, and W. Wegscheider, *Phys. Rev. B* **90**, 205309 (2014).
- [60] S. Gambino, M. Mazzeo, A. Genco, O. Di Stefano, S. Savasta, S. Patanè, D. Ballarini, F. Mangione, G. Lervario, D. Sanvitto, and G. Gigli, *ACS Photonics* **1**, 1042 (2014).
- [61] R. Chikkaraddy, B. de Nijs, F. Benz, S. J. Barrow, O. A. Scherman, E. Rosta, A. Demetriadou, P. Fox, O. Hess, and J. J. Baumberg, *Nature* **535**, 127 (2016).
- [62] F. Yoshihara, T. Fuse, S. Ashhab, K. Kakuyanagi, S. Saito, and K. Semba, *Nat. Phys.* **13**, 44 (2017).
- [63] A. Bayer, M. Pozimski, S. Schambeck, D. Schuh, R. Huber, D. Bougeard, and C. Lange, *Nano Lett.* **17**, 6340 (2017).
- [64] M. Halbhuber, J. Mornhinweg, V. Zeller, C. Ciuti, D. Bougeard, R. Huber, and C. Lange, *Nat. Photon.* **14**, 675 (2020).
- [65] A. Genco, A. Ridolfo, S. Savasta, S. Patanè, G. Gigli, and M. Mazzeo, *Adv. Opt. Mater.* **6**, 1800364 (2018).
- [66] J. Flick, M. Ruggenthaler, H. Appel, and A. Rubio, *PNAS* **114**, 3026 (2017).
- [67] P. Forn-Díaz, L. Lamata, E. Rico, J. Kono, and E. Solano, *Rev. Mod. Phys.* **91**, 025005 (2019).
- [68] A. Frisk Kockum, A. Miranowicz, S. De Liberato, S. Savasta, and F. Nori, *Nat. Rev. Phys.* **1**, 19 (2019).
- [69] H. Hübener, U. De Giovannini, C. Schäfer, J. Andberger, M. Ruggenthaler, J. Faist, and A. Rubio, *Nat. Mater.* **20**, 438 (2021).
- [70] M. Ruggenthaler, N. Tancogne-Dejean, J. Flick, H. Appel, and A. Rubio, *Nat Rev Chem* **2**, 1 (2018).
- [71] J. Flick, D. M. Welakuh, M. Ruggenthaler, H. Appel, and A. Rubio, *ACS Photonics* **6**, 2757 (2019).
- [72] N. S. Mueller, Y. Okamura, B. G. M. Vieira, S. Juergensen, H. Lange, E. B. Barros, F. Schulz, and S. Reich, *Nature* **583**, 780 (2020).
- [73] J. C. Owens, M. G. Panetta, B. Saxberg, G. Roberts, S. Chakram, R. Ma, A. Vrajitoarea, J. Simon, and D. I. Schuster, *Nat. Phys.* , 1 (2022).
- [74] Y. Ashida, T. Yokota, A. İmamoğlu, and E. Demler, *Phys. Rev. Res.* **4**, 023194 (2022).
- [75] T. W. Ebbesen, *Acc. Chem. Res.* **49**, 2403 (2016).
- [76] J. Feist, J. Galego, and F. J. Garcia-Vidal, *ACS Photonics* **5**, 205 (2018).
- [77] R. F. Ribeiro, L. A. Martínez-Martínez, M. Du, J. Campos-Gonzalez-Angulo, and J. Yuen-Zhou, *Chem. Sci.* **9**, 6325 (2018).
- [78] J. Galego, F. J. Garcia-Vidal, and J. Feist, *Phys. Rev. X* **5**, 041022 (2015).
- [79] F. J. Garcia-Vidal, C. Ciuti, and T. W. Ebbesen, *Science* **373**, eabd0336 (2021).
- [80] F. Schlawin, D. M. Kennes, and M. A. Sentef, *Appl. Phys. Rev.* **9**, 011312 (2022).
- [81] J. Bloch, A. Cavalleri, V. Galitski, M. Hafezi, and A. Rubio, *Nature* **606**, 41 (2022).
- [82] E. Orgiu, J. George, J. A. Hutchison, E. Devaux, J. F. Dayen, B. Doudin, F. Stellacci, C. Genet, J. Schachenmayer, C. Genes, G. Pupillo, P. Samorì, and T. W. Ebbesen, *Nature Mater.* **14**, 1123 (2015).
- [83] H. Konishi, K. Roux, V. Helson, and J.-P. Brantut, *Nature* **596**, 509 (2021).
- [84] P. Pilar, D. D. Bernardis, and P. Rabl, *Quantum* **4**, 335 (2020).
- [85] J. Román-Roche and D. Zueco, *SciPost Phys. Lect. Notes* , 50 (2022).
- [86] Z. Zhang, H. Hirori, F. Sekiguchi, A. Shimazaki, Y. Iwasaki, T. Nakamura, A. Wakamiya, and Y. Kanemitsu, *Phys. Rev. Res.* **3**, L032021 (2021).
- [87] D. M. Juraschek, T. Neuman, J. Flick, and P. Narang, *Phys. Rev. Res.* **3**, L032046 (2021).
- [88] K. Lenk, J. Li, P. Werner, and M. Eckstein, *arXiv:2205.05559* (2022).
- [89] Y. Ashida, A. İmamoğlu, J. Faist, D. Jaksch, A. Cavalleri, and E. Demler, *Phys. Rev. X* **10**, 041027 (2020).
- [90] S. Latini, D. Shin, S. A. Sato, C. Schäfer, U. De Giovannini, H. Hübener, and A. Rubio, *PNAS* **118**, e2105618118 (2021).
- [91] C.-R. Mann, T. J. Sturges, G. Weick, W. L. Barnes, and E. Mariani, *Nat. Commun.* **9**, 2194 (2018).
- [92] X. Wang, E. Ronca, and M. A. Sentef, *Phys. Rev. B* **99**, 235156 (2019).
- [93] V. Rokaj, M. Penz, M. A. Sentef, M. Ruggenthaler, and A. Rubio, *Phys. Rev. Lett.* **123**, 047202 (2019); *Phys. Rev. B* **105**, 205424 (2022).
- [94] C. A. Downing, T. J. Sturges, G. Weick, M. Stobińska, and L. Martín-Moreno, *Phys. Rev. Lett.* **123**, 217401 (2019).
- [95] I. V. Tokatly, D. R. Gulevich, and I. Iorsh, *Phys. Rev. B* **104**, L081408 (2021).
- [96] K. Masuki and Y. Ashida, *Phys. Rev. B* **107**, 195104 (2023).
- [97] M. A. Sentef, M. Ruggenthaler, and A. Rubio, *Sci. Adv.* **4**, eaau6969 (2018).
- [98] F. Schlawin, A. Cavalleri, and D. Jaksch, *Phys. Rev. Lett.* **122**, 133602 (2019).
- [99] J. B. Curtis, Z. M. Raines, A. A. Allocca, M. Hafezi, and V. M. Galitski, *Phys. Rev. Lett.* **122**, 167002 (2019).
- [100] J. B. Curtis, A. Grankin, N. R. Poniatowski, V. M. Galitski, P. Narang, and E. Demler, *Phys. Rev. Res.* **4**, 013101 (2022).
- [101] J. Li, L. Schamriß, and M. Eckstein, *Phys. Rev. B* **105**, 165121 (2022).
- [102] A. Thomas, E. Devaux, K. Nagarajan, G. Rogez, M. Seidel, F. Richard, C. Genet, M. Drillon, and T. W. Ebbesen, *Nano Lett.* **21**, 4365 (2021).
- [103] M. Kiffner, J. R. Coulthard, F. Schlawin, A. Ardavan, and D. Jaksch, *Phys. Rev. B* **99**, 085116 (2019); M. Kiffner, J. Coulthard, F. Schlawin, A. Ardavan, and

- D. Jaksch, *New Journal of Physics* **21**, 073066 (2019).
- [104] A. Chiocchetta, D. Kiese, C. P. Zelle, F. Piazza, and S. Diehl, *Nat. Commun.* **12**, 5901 (2021).
- [105] J. Li, D. Golez, G. Mazza, A. J. Millis, A. Georges, and M. Eckstein, *Phys. Rev. B* **101**, 205140 (2020).
- [106] E. Vinas Boström, A. Sriram, M. Claassen, and A. Rubio, *arXiv:2211.07247* (2022).
- [107] S. Smolka, W. Wuester, F. Haupt, S. Faelt, W. Wegscheider, and A. Imamoglu, *Science* **346**, 332 (2014).
- [108] Q. Zhang, M. Lou, X. Li, J. L. Reno, W. Pan, J. D. Watson, M. J. Manfra, and J. Kono, *Nat. Phys.* **12**, 1005 (2016).
- [109] G. L. Paravicini-Bagliani, F. Appugliese, E. Richter, F. Valmorra, J. Keller, M. Beck, N. Bartolo, C. Rössler, T. Ihn, K. Ensslin, C. Ciuti, G. Scalari, and J. Faist, *Nat. Phys.* **15**, 186 (2019).
- [110] J. Keller, G. Scalari, F. Appugliese, S. Rajabali, M. Beck, J. Haase, C. A. Lehner, W. Wegscheider, M. Failla, M. Myronov, D. R. Leadley, J. Lloyd-Hughes, P. Nataf, and J. Faist, *Phys. Rev. B* **101**, 075301 (2020).
- [111] F. Appugliese, J. Enkner, G. L. Paravicini-Bagliani, M. Beck, C. Reichl, W. Wegscheider, G. Scalari, C. Ciuti, and J. Faist, *Science* **375**, 1030 (2022).
- [112] S. Ravets, P. Knüppel, S. Faelt, O. Cotlet, M. Kroner, W. Wegscheider, and A. Imamoglu, *Phys. Rev. Lett.* **120**, 057401 (2018).
- [113] D. Hagenmüller, S. De Liberato, and C. Ciuti, *Phys. Rev. B* **81**, 235303 (2010).
- [114] M. Devoret, S. Girvin, and R. Schoelkopf, *Ann. Phys.* **519**, 767 (2007).
- [115] Y. Ashida, A. m. c. İmamoğlu, and E. Demler, *Phys. Rev. Lett.* **130**, 216901 (2023).
- [116] Z. Jacob, *Nat. Mater.* **13**, 1081 (2014).
- [117] P. Törmä, S. Peotta, and B. A. Bernevig, *Nat. Rev. Phys.* **4**, 528 (2022).
- [118] G. E. Topp, C. J. Eckhardt, D. M. Kennes, M. A. Sentef, and P. Törmä, *Phys. Rev. B* **104**, 064306 (2021).
- [119] A. H. MacDonald, S. M. Girvin, and D. Yoshioka, *Phys. Rev. B* **37**, 9753 (1988).
- [120] D. P. Arovas, E. Berg, S. A. Kivelson, and S. Raghu, *Annu. Rev. Condens. Matter Phys.* **13**, 239 (2022).
- [121] Z. Zhu and S. R. White, *Phys. Rev. B* **92**, 041105 (2015).
- [122] S.-S. Gong, W. Zheng, M. Lee, Y.-M. Lu, and D. N. Sheng, *Phys. Rev. B* **100**, 241111 (2019).
- [123] S. Hu, W. Zhu, S. Eggert, and Y.-C. He, *Phys. Rev. Lett.* **123**, 207203 (2019).
- [124] A. Szasz, J. Motruk, M. P. Zaletel, and J. E. Moore, *Phys. Rev. X* **10**, 021042 (2020).
- [125] M. Drescher, L. Vanderstraeten, R. Moessner, and F. Pollmann, *arXiv:2209.03344* (2022).
- [126] J. D. Caldwell, A. V. Kretinin, Y. Chen, V. Giannini, M. M. Fogler, Y. Francescato, C. T. Ellis, J. G. Tischler, C. R. Woods, A. J. Giles, M. Hong, K. Watanabe, T. Taniguchi, S. A. Maier, and K. S. Novoselov, *Nat. Commun.* **5**, 1 (2014).
- [127] S. Dai, Z. Fei, Q. Ma, A. S. Rodin, M. Wagner, A. S. McLeod, M. K. Liu, W. Gannett, W. Regan, K. Watanabe, T. Taniguchi, M. Thiemens, G. Dominguez, A. H. C. Neto, A. Zettl, F. Keilmann, P. Jarillo-Herrero, M. M. Fogler, and D. N. Basov, *Science* **343**, 1125 (2014).
- [128] A. J. Giles, S. Dai, I. Vurgaftman, T. Hoffman, S. Liu, L. Lindsay, C. T. Ellis, N. Assefa, I. Chatzakis, T. L. Reinecke, J. G. Tischler, M. M. Fogler, J. H. Edgar, D. N. Basov, and J. D. Caldwell, *Nat. Mater.* **17**, 134 (2018).
- [129] S. Dai, W. Fang, N. Rivera, Y. Stehle, B.-Y. Jiang, J. Shen, R. Y. Tay, C. J. Ciccarino, Q. Ma, D. Rodan-Legrain, P. Jarillo-Herrero, E. H. T. Teo, M. M. Fogler, P. Narang, J. Kong, and D. N. Basov, *Adv. Mater.* **31**, 1806603 (2019).
- [130] E. Y. Ma, J. Hu, L. Waldecker, K. Watanabe, T. Taniguchi, F. Liu, and T. F. Heinz, *Nano Lett.* **22**, 8389 (2022).
- [131] H. H. Sheinfux, L. Orsini, M. Jung, I. Torre, M. Cecchetti, R. Maniyara, D. B. Ruiz, A. Hötger, R. Bertini, S. Castilla, N. C. H. Hesp, E. Janzen, A. Holleitner, V. Pruneri, J. H. Edgar, G. Shvets, and F. H. L. Koppens, *arXiv:2202.08611* (2022).
- [132] See Supplementary Materials for further details on the statements and the derivations.
- [133] D. Xiao, G.-B. Liu, W. Feng, X. Xu, and W. Yao, *Phys. Rev. Lett.* **108**, 196802 (2012).
- [134] C. Zhang, C. Gong, Y. Nie, K.-A. Min, C. Liang, Y. J. Oh, H. Zhang, W. Wang, S. Hong, L. Colombo, R. M. Wallace, and K. Cho, *2D Mater.* **4**, 015026 (2016).
- [135] Y. Wang, T. Shi, and C.-C. Chen, *Phys. Rev. X* **11**, 041028 (2021).
- [136] Y. Ashida, A. İmamoğlu, and E. Demler, *Phys. Rev. Lett.* **126**, 153603 (2021).
- [137] M. Liao, Z. Wei, L. Du, Q. Wang, J. Tang, H. Yu, F. Wu, J. Zhao, X. Xu, B. Han, *et al.*, *Nat. Commun.* **11**, 2153 (2020).
- [138] L. Zhang, Z. Zhang, F. Wu, D. Wang, R. Gogna, S. Hou, K. Watanabe, T. Taniguchi, K. Kulkarni, T. Kuo, *et al.*, *Nat. Commun.* **11**, 5888 (2020).
- [139] S. Tao, X. Zhang, J. Zhu, P. He, S. A. Yang, Y. Lu, and S.-H. Wei, *J. Am. Chem. Soc.* **144**, 3949 (2022).